



1 SARAH-3 – satellite-based climate data records of surface solar radiation

2 Uwe Pfeifroth, Jaqueline Drücke, Steffen Kothe, Jörg Trentmann, Marc Schröder and Rainer Hollmann
3 Deutscher Wetterdienst, satellite-based climate monitoring, Offenbach, Germany

4 Correspondence: Uwe Pfeifroth (uwe.pfeifroth@dwd.de)

6 Abstract

7 The amount of energy reaching the Earth's surface from the sun is a quantity of high importance for the climate system and
8 for renewable energy applications. SARAH-3 is a new edition of a satellite-based climate data record of surface solar radiation
9 parameters. It is generated and distributed by the European Organisation of Meteorological Satellites (EUMETSAT) Satellite
10 Application Facility on Climate Monitoring (CM SAF). SARAH-3 covers more than 4 decades of data and provides a high
11 spatial resolution of $0.05^\circ \times 0.05^\circ$ and a temporal resolution of 30-minutes, daily means and monthly means. SARAH-3 consists
12 of seven parameters including surface irradiance, direct irradiance and sunshine duration. SARAH-3 is the successor of
13 SARAH-2.1 and is accompanied by an operational near-real time processing of all parameters – the so-called Interim Climate
14 Data Record, enabling climate monitoring applications. The validation of SARAH-3 shows a good accuracy and stability of
15 the data record and further improves over its predecessor. One reason for this improvement is the new treatment of snow-
16 covered surfaces in the algorithm, reducing the misclassification of snow as clouds. The SARAH-3 climate analysis reveals
17 an increase of the surface irradiance during the last decades in Europe.

18 1 Introduction

19 Surface solar radiation is of high importance for the Earth's climate (Ramanathan et al. 2001, Wild et al., 2012) and for life on
20 Earth in general. Beside the astronomical Earth-Sun constellation and the individual daytime and location, surface solar
21 radiation (SSR) is controlled by the atmospheric and surface properties. Overall, an important factor influencing SSR are
22 clouds, which strongly reflect solar radiation / reduce SSR and are highly variable in space and time (Pfeifroth et al., 2018,
23 Wild, 2012, Hartmann et al., 1986). Hence a dense observational network is required to capture the temporal and spatial
24 variability of SSR. However, station-based high quality SSR measurements are often available only at relatively few stations,
25 e.g. from the Baseline Surface Radiation Network (BSRN), which do not capture neither the global nor regional SSR spatial
26 and temporal distributions appropriately. Large gaps in space and time exist in the surface network, especially over the ocean
27 and on the African continent.

28 Satellite data have become a valuable data source to fill the gaps (e.g. Gautier et al., 1980, Pinker et al., 1992) – not only in
29 space, but also in time. SSR has been estimated from satellite measurements since the 1980s using a range of different retrieval
30 methods (Rigollier et al., 2004; Vernay et al., 2004; Möser and Raschke, 1984; Cano et al., 1986; Müller et al., 2015, 2022).
31 The generation of longer-term data records, however, has only been started in the 2000s, when higher quality satellite data
32 became available for one decade or longer. The data used for the monitoring of the climate typically is required to cover
33 multiple decades (i.e., 20 years or more) and to be temporally homogeneous, in addition to have a high accuracy.

34 Here we are presenting the climate data record (CDR) SARAH-3 (Pfeifroth et al., 2023,
35 https://doi.org/10.5676/EUM_SAF_CM/SARAH/V003) generated by EUMETSAT's Climate Monitoring Satellite
36 Application Facility (CM SAF, Schulz et al., 2009), i.e., the latest version of the series of SARAH CDRs. SARAH-3 has been
37 released in May 2023 and covers more than 40 years (1983 to date), including, for the first time, the current WMO climate
38 normal period: 1991-2020. SARAH-3 provides seven surface solar radiation parameters: solar irradiance (also called global
39 radiation), two direct irradiance parameters (horizontal and normal), sunshine duration, two spectral surface radiation
40 parameter (i.e. PAR, DAL) and the effective cloud albedo.

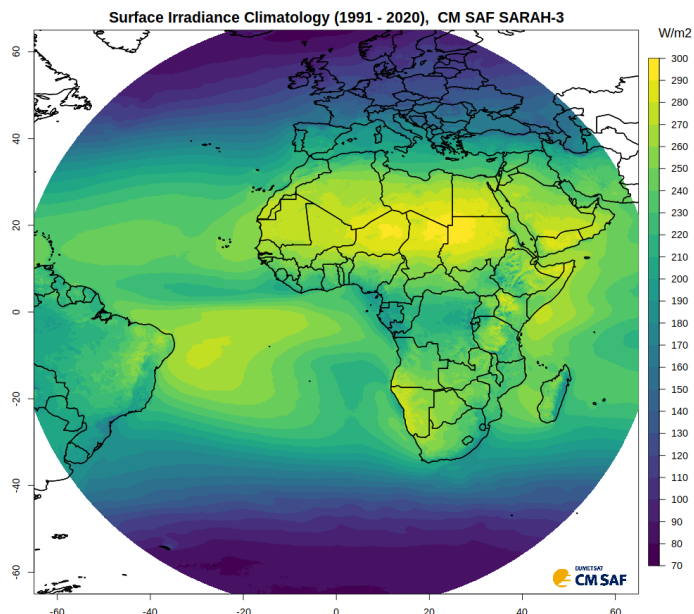


41 SARAH stands for ‘SurfAce Radiation DATaset Heliosat’. The data are based on the series of the geostationary METEOSAT
42 Satellites of the first and second generation. The first METEOSAT-based SSR data record has been released by CM SAF more
43 than a decade ago (Posselt et al, 2011) and with its successors SARAH-1, SARAH-2 and SARAH-2.1 the generated data have
44 been steadily improved and extended in time. While for SARAH-1, the main step was the inclusions of the MVIRI sensor
45 (onboard the 1st METEOSAT generation) and the SEVIRI sensor (onboard the 2nd METEOSAT generation) (Müller et al.,
46 2015), the stability over time was further improved with SARAH-2 (covering 1983-2015). SARAH-2.1 is the extension of the
47 SARAH-2 CDR and came with a near-realtime processing for the first time. The so-called Interim Climate Data Records
48 (ICDR) operationally, consistently extended the SARAH-2 CDR with a short delay of 2-3 days. The current SARAH edition,
49 SARAH-3, is also accompanied and temporally extended by ICDR data, which enables climate monitoring applications (e.g.
50 C3S, 2023). The main conceptional improvement in the generation of SARAH-3 has been the improved estimation of the
51 surface solar radiation parameters in case of snow-covered surfaces, which reduced the underestimation of surface solar
52 radiation and sunshine duration found in previous editions of SARAH (e.g., Niermann et al., 2019). Two novel parameters,
53 representing different spectral regions, are included in SARAH-3, namely Daylight (DAL) and Photosynthetic Active
54 Radiation (PAR).

55 All CM SAF data records are freely available without restrictions via the CM SAF Web User Interface (see www.cmsaf.eu,
56 wui.cmsaf.eu) in NetCDF-format. The previous editions of the SARAH climate data records are already widely used in many
57 fields and applications, including climate analysis (e.g. Pfeifroth et al., 2018), climate monitoring (e.g. C3S, 2023), renewable
58 energy (Drücke et al., 2021, Kaspar et al., 2019), model evaluation (e.g. Alexandri et al., 2015), agrometeorology and biology
59 (e.g. Pelosi et al., 2022), data fusion (e.g. Zak et al., 2015), and quality control of station data (e.g. Urraca et al., 2017, 2020).
60 This article provides an overview of the most important aspects of the CM SAF SARAH-3 climate data record. The retrieval
61 algorithm is described in section 2. Section 3 presents the validations of the data record and in section 4 some example
62 applications of the SARAH-3 data record are given. Data availability is described in section 5. Finally, summary and
63 conclusions are presented in section 6.

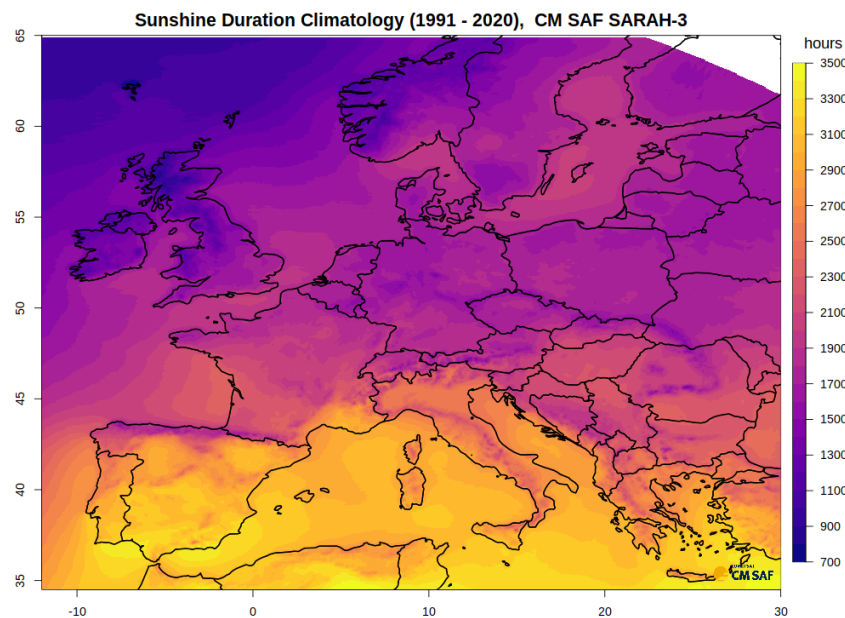
64 **2 SARAH-3 parameters and retrieval method**

65 SARAH-3 is a climate data record generated and distributed by the EUMETSAT Satellite Application Facility on Climate
66 Monitoring (CM SAF). It is the latest edition of SARAH data records and is based on instruments onboard the series of
67 METEOSAT geostationary satellites including the first (MFG) and second (MSG) generations. SARAH-3 thereby combines
68 the MVIRI instruments (on MFG) and the SEVIRI instruments (on MSG) sensors and covers the time period from 1983 to
69 date. The data record covers the region from 65°S to 65°N and from 65°W to 65°E (see Figure 1) and is provided on a regular
70 0.05° x 0.05° grid. The available temporal resolutions are 30-minutes (instantaneous), daily and monthly means. Figure 2
71 shows the sunshine duration climatology for Europe. The annual sunshine duration in Europe varies between less than 1000
72 hours in the North and more than 3000 hours in the Mediterranean area. The parameters included in SARAH-3 are presented
73 in Table 1.



74

75 **Figure 1: SARA3 surface irradiance climatology for the climate normal period (1991-2020).**



76

77 **Figure 2: SARA3 sunshine duration mean annual sum for Europe, for the climate normal period (1991-2020).**

SARA3 Parameter	Abbreviation	Unit
Surface Irradiance (Global Radiation)	SIS	W/m^2
Surface Direct Irradiance	SID	W/m^2
Direct Normal Irradiance	DNI	W/m^2
Photosynthetic Active Radiation	PAR	$\mu mol/(m^2 * s)$



Daylight	DAL	kLux
Effective Cloud Albedo	CAL	-
Sunshine Duration	SDU	hours

78 **Table 1: Parameters, abbreviations and units included in SARAH-3.**

79 The retrieval method to estimate surface solar radiation used for the generation of all editions of the SARAH data record is
80 based on the Heliosat-approach (Cano et al., 1986; Hammer et al., 2003) and is described in detail in Müller et. al, 2015 and
81 further put into perspective in Müller et al., 2023. In brief, the method is a two-step approach: First the Effective Cloud Albedo
82 (CAL) is derived from the visible satellite data, in a second step CAL is used together with a clear-sky surface solar radiative
83 transfer model to derive the all-sky surface solar radiation parameters. The estimation of the clear-sky surface solar radiation
84 requires some auxiliary data (see section 2.5).

85 One main new implementation in the SARAH-3 retrieval scheme compared to previous editions of SARAH is the improved
86 consideration of snow-covered surfaces by internally detecting snow-covered surfaces (see Section 2.1). This information is
87 used as part of the Heliosat-algorithm to generate a more accurate Effective Cloud Albedo in the case of snow-covered surfaces.
88 By combining the SPECMAGIC clear-sky model (see Section 2.2) with CAL, the all-sky surface solar radiation parameters
89 are derived (see Section 2.3). Section 2.4 introduces the sunshine duration parameter and its retrieval algorithm based on the
90 direct normal irradiance (DNI). For the estimation of the clear-sky surface solar radiation using a radiative transfer model some
91 auxiliary data are required and described in Section 2.5. The estimation of daily and monthly averages from the instantaneous
92 satellite retrievals is presented in Section 2.6.

93 **2.1 Heliosat - HelSnow**

94 Data from the previous editions of the SARAH data records suffered from occasional misclassifications of snow-covered
95 surfaces as clouds, which resulted in a too high effective cloud albedo (CAL), in particular under predominantly clear-sky,
96 snow-covered conditions, and subsequently in significant underestimations of surface solar radiation (Niermann et al., 2019).
97 With the help of HelSnow, the data quality has improved considerably under such conditions in SARAH-3 (see Section 3.2).
98 With SARAH-3, the classical Heliosat approach to generate CAL is extended by the so-called HelSnow-algorithm. The
99 HelSnow-algorithm is applied to estimate the surface reflectance (ρ_{\min}) in the presence of snow before the application of
100 the ‘classical’ Heliosat-algorithm. The snow detection in HelSnow is a novel method to efficiently distinguish between clouds
101 and snow-covered surfaces based on the detection of moving bright objects. This method takes advantage of the high temporal
102 frequency of observations from geostationary satellites and from the fact that clouds typical move in time, while snow-covered
103 surfaces are immobile. The HelSnow-method is able to separate snow and cloud coverage based on data from only the
104 satellite’s visible channel, allowing the consistent processing across multiple generations of satellite instruments.

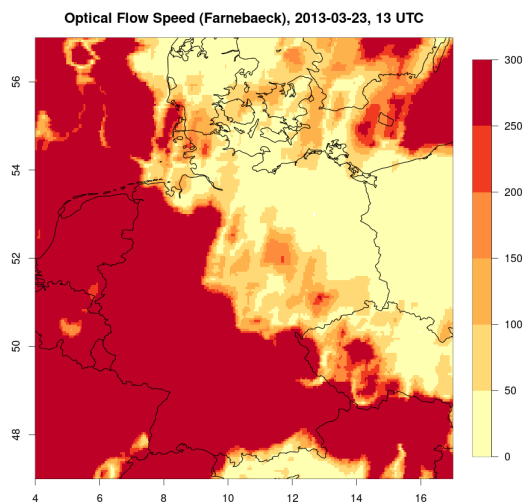
105 The basic assumption for snow detection in HelSnow is rather simple: Bright areas that are in motion are considered being
106 cloudy; bright regions without motion may be snow-covered surfaces. As the final result, daily information of snow-covered
107 surfaces and their daily-averaged brightness is generated, which is used subsequently in the estimation of the effective cloud
108 albedo. There are four main steps in the implementation of the HelSnow-algorithm to generate daily snow brightness data,
109 which is subsequently used in the Heliosat-approach.

110 **2.1.1 Step 1: Detection of motion**

111 Using the ‘Farnebaeck’-algorithm (Farneböck, 2003) in standard settings, ‘motion’ is detected in a sequence of two images
112 (technically the OpenCV software library is used, see <https://opencv.org/>). If the speed of the motion is lower than a certain
113 threshold, the pixel (or objects of several pixels) is potentially cloud-free. This threshold is different for the MVIRI and SEVIRI
114 sensors (i.e. 160 and 112, respectively) due to the different native spatial resolutions of the sensors. An example of the
115 Farnebaeck speed is shown in Figure 3. All pixels with motion levels above / below the specified threshold are considered in



116 motion and not in motion, respectively. Only those pixels below the threshold, i.e., those determined to be not in motion, hence
117 being cloud-free, are further considered.

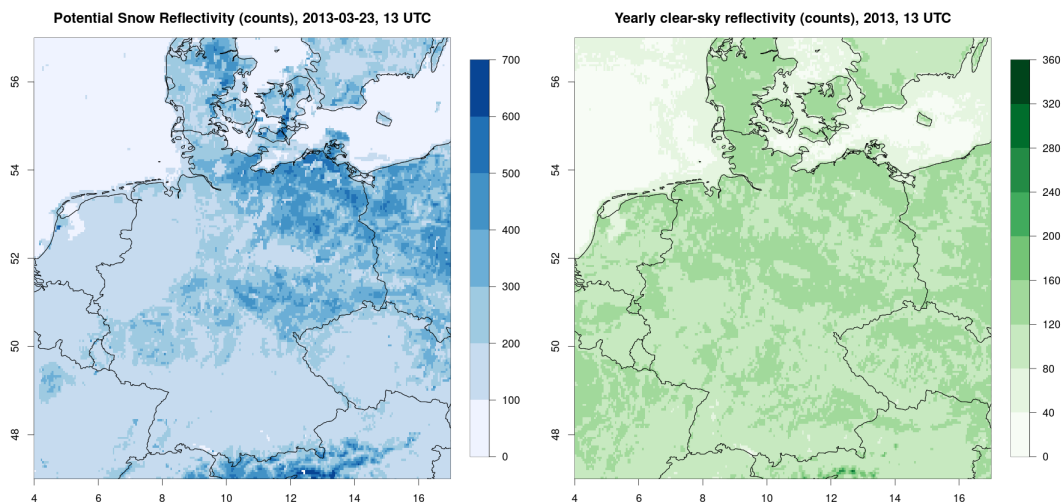


118
119 **Figure 3: Optical Flow speed (unitless) derived by the Farnebaeck algorithm for 2013-03-23, 13 UTC.**

120 **2.1.2 Step 2: Detection of sub-daily snow**

121 In the second step of the HelSnow algorithm potentially snow-covered surfaces are identified for every 30-min satellite slot
122 between 0900 UTC and 1530 UTC. For all pixels identified as not-in-motion, i.e., cloud-free, in step 1 the difference between
123 the actual measured reflectivity and a reference clear-sky is calculated. In case this difference is larger (i.e., the pixel is brighter)
124 than a predefined threshold the corresponding satellite pixel is considered snow-covered for this time step / satellite slot,
125 otherwise this pixel is considered snow-free. The reference clear-sky value is calculated for each year based on the individual
126 satellite slots and based on the months of June, July and August. This calculation is done for each year to account for different
127 instrument calibrations and degradations. For the ICDR (2021 onwards) the clear-sky values for 2020 are used, as the SEVIRI
128 instruments are quite stable over time.

129 In case of clouds (i.e., ‘motion’ is detected in step 1) the view onto the Earth’s surface is not possible, in this case, the last
130 valid observation of the surface for the corresponding satellite slot (e.g. the 1300 UTC slot) (either snow-covered surface or
131 not snow-covered surface) is kept unchanged from the same satellite slot from the previous day. This step is performed for
132 each available satellite measurement between 0900 and 1530 UTC. An example of the instantaneous (snow) reflectivity for
133 2013-03-23, 13 UTC is shown in Figure 4 (left). The corresponding clear-sky reference value to which the values from the
134 determined clear-sky pixels are compared to, is shown in Figure 4 (right). Note that the reflectivities of snow-covered surfaces
135 typically are substantially larger than those of the reference surface reflectivities. The corresponding threshold used to separate
136 snow-covered surfaces from non-snow-covered surfaces is set to 60 counts.

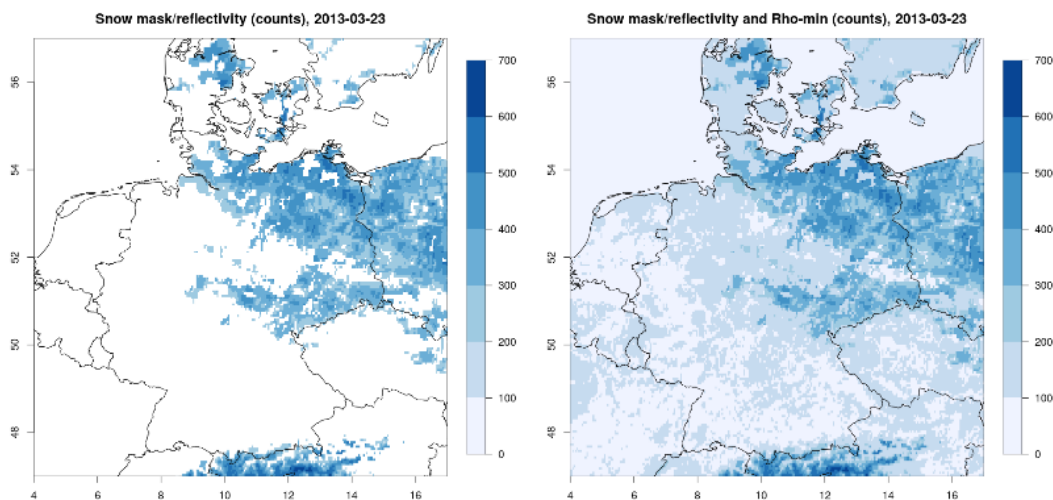


137

138 **Figure 4: Example of an instantaneous (potentially snow) reflectivity (left) for 2013-03-23, 13 UTC, and the corresponding clear-sky**
139 **background reference reflectivity (right) for 2013, 13 UTC (note the different ranges of the color scales).**

140 2.1.3 Step 3: Derivation of the daily snow brightness data

141 Using the sub-daily (30-min instantaneous) information on potentially snow-covered pixels, pixels are classified as snow-
142 covered for that particular day if the pixels have been classified as snow-covered (in step 2) for more than 2/3 of the used
143 daytime observations. In this case, the associated clear sky reflection (ρ_{\min}) for these pixels are derived as the temporal
144 average of the instantaneous clear-sky reflections for the particular day. As a final step, to minimize incorrectly classified
145 snow-covered surfaces (e.g. during fog events), the daily snow-coverage information is corrected using snow and sea ice
146 coverage data from ECMWF global analysis data records (see Section 2.5.1). That means snow-covered surfaces as detected
147 from the satellite observations are not treated as snow-covered if there is no snow in the reanalysis data. Figure 5 (left) shows
148 the final daily snow mask / snow reflectivity on 2013-03-13.



149

150 **Figure 5: Daily snow mask/reflectivity (left) and the combined snow mask and ρ_{\min} data (2013-03, 13 UTC) (right) used for the**
151 **derivation of CAL for 2013-03-23.**



152 2.1.4 Step 4: Heliosat with snow data

153 The final step of the HelSnow-Heliosat-approach generates the Effective Cloud Albedo (CAL) based on a monthly statistic of
154 satellite images (see also Müller et al., 2015). The basic formula is $CAL = \frac{\rho - \rho_{min}}{\rho_{max} - \rho_{min}}$, ρ is the actual radiance measured by the
155 sensor, ρ_{min} is the clear-sky reflectance estimated as the minimum reflectance over a certain period of time and derived for
156 each satellite slot to consider the directional surface reflectance. In the case a snow-covered surface was detected by the
157 HelSnow-approach (i.e., 66% of the available satellite slots have been clear-sky and snow-covered, allowing the update of the
158 snow-reflectivity in step 3) the daily clear-sky reflectivity is used for all satellite slots. This implies that the high values of the
159 snow- ρ_{min} are only used under (mostly) clear-sky conditions and prevents the degradation of the sensitivity of the Heliosat-
160 approach under cloudy and snow-covered conditions. ρ_{max} is the maximum reflectance determined per month as derived by
161 the 95th percentile of the values in a region in the south Atlantic Ocean with a frequent occurrence of clouds (see also Müller
162 et al., 2015). ρ_{max} normalizes the cloud albedo and considers the different sensitivities of the satellite instruments and the
163 degradation of the sensor sensitivity in time. Finally, this leads to enhanced temporal stability of the data record.
164 The result of the HelSnow-Heliosat-algorithm is CAL, which is the normalized cloud reflectivity relative to the clear-sky
165 reflectance, now considering snow-covered surfaces. CAL is used subsequently as the main input for the calculation of the
166 surface solar radiation parameters.

167 2.2 SPECMAGIC

168 The SPECMAGIC (Spectral Mesoscale Global Irradiance Code) clear-sky surface solar radiation model is used to estimate
169 the total and direct clear-sky surface irradiance (Müller et al., 2012; 2015). SPECMAGIC applies an efficient hybrid-
170 eigenvector Look-Up-Table (LUT) approach based on the modified Lambert Beer function (MLB) (Mueller et al., 2004, 2009,
171 2012) to allow the efficient processing of long-term satellite data. The LUT has been generated using the libRadtran RTM
172 (Mayer et al., 2005). It has been derived for fixed values of integrated ozone, integrated water vapor and surface albedo, two
173 solar zenith angles, and a large range of aerosol properties. SPECMAGIC provides clear-sky surface solar radiation for 32
174 spectral bands (so-called Kato-bands, see Kato et al., 1999). For more information the reader is referred to Mueller et al., 2012,
175 2015.

176 For the calculation of the clear-sky surface solar radiation auxiliary data is required. A description of the auxiliary data used
177 for the generation of SARA3-3 is presented in Section 2.5.

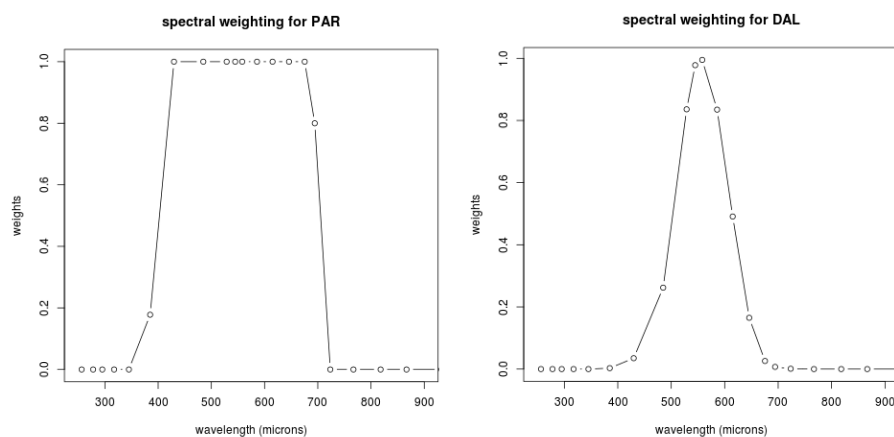
178 The total and the direct clear-sky surface irradiance are derived as the sum of the irradiances of the 32 spectral Kato-bands.
179 The clear-sky surface solar radiation for the spectral parameters, PAR and DAL, are derived according to their definitions (see
180 Alados et al., 1995 and <https://cie.co.at/>) by adding the weighted irradiances from the corresponding spectral Kato-bands.
181 Figure 6 shows the weighting of the Kato-bands for the estimation of PAR and DAL. The broadband parameters (SIS, SID,
182 DNI) are calculated by summing up the respective spectral irradiances from all Kato-bands.

183 2.3 All Sky Radiation

184 The all-sky surface solar radiation is derived by combining the effective cloud albedo derived from the satellite data and the
185 clear-sky surface solar radiation estimated using SPECMAGIC. The clear-sky index, k , is defined as the ratio between the all-
186 sky radiation I and the clear-sky radiation I_{clr} : $k = I / I_{clr}$; hence the all-sky surface irradiance is estimated as $I = k * I_{clr}$.
187 For the estimation of the surface direct irradiance, the following relation is used: $SID = SID_{clear}(k - 0.38 \cdot (1 - k))^{2.5}$
188 The clear-sky index k , can be estimated from the effective cloud albedo using the Heliosat-relation (Hammer et al., 2003);
189 over wide ranges of CAL ($-0.05 < CAL < 0.8$) the relation between k and CAL is $k = 1 - CAL$, which provides, multiplied by
190 I_{clr} , the estimate of the all-sky surface irradiance: $I = (1 - CAL) * I_{clr}$. To estimate the clear-sky index outside this range of
191 CAL other relations between CAL and k are used (Mueller et al., 2015).



192 Spectral effects of clouds are also considered resulting in a spectral adjustment of the clear-sky index, requiring the separate
 193 estimation of the all-sky surface for each individual Kato-band using the spectrally dependent clear-sky index and clear-sky
 194 irradiance. For further information on the estimation of the spectrally-resolved all-sky surface solar radiation parameters see
 195 Müller et al., 2012, 2015.
 196 The final all-sky irradiance is estimated as the sum of the spectral all-sky irradiances for the corresponding spectral Kato bands,
 197 as described in the previous Section. The Direct Normal Irradiance (DNI) is calculated by $DNI = SID * \cos(SZA)$, where
 198 SZA is the Sun Zenith Angle.



199
 200 **Figure 6: Spectral weighting for the SARAH-3 parameters Photosynthetic Active Radiation (PAR) and Daylight (DAL).**

201 **2.4 Sunshine Duration**

202 Basis for the retrieval of the SARAH-3 SDU data record is the instantaneous (30 minutes) Direct Normal Irradiance (DNI)
 203 data and the WMO threshold for sunshine, which is defined by $DNI \geq 120 W/m^2$. In SARAH-3 the maximum possible daily
 204 sunshine duration is determined using the 2.5° threshold for the solar elevation angle and the $120 W/m^2$ for the DNI. Here, the
 205 solar elevation angle under clear-sky condition is used and if it falls below the threshold of 2.5° , it is set to exactly the angle
 206 where $120 W/m^2$ is reached. SDU is derived by the ratio of the number of “sunny” satellite slots to all available slots during
 207 daylight multiplied with the theoretically possible daylength:

208
$$SDU = \text{daylength} * \frac{\sum_{i=1}^{\text{iday}} (W_i(\text{sunny_slot}_i))}{\#\text{daylight_slots}}$$

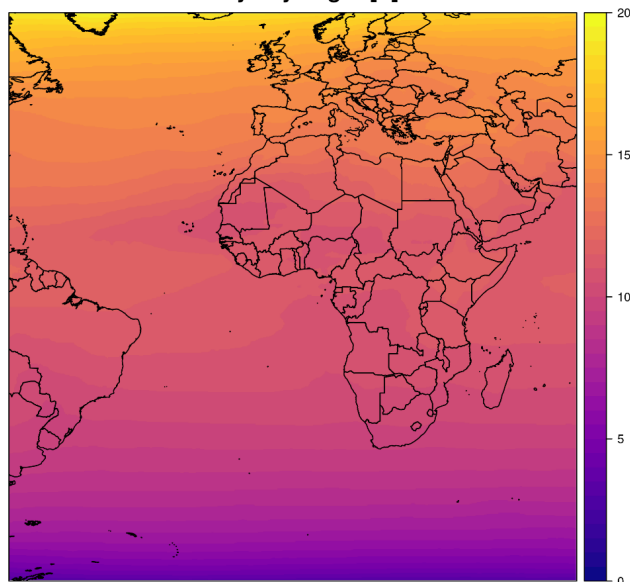
209 The theoretically daylength is pre-calculated depending on the date and location using the simplified SOLIS clear sky radiation
 210 model to estimate clear sky DNI (see Ineichen, 2008, Antonanzas-Torres et al., 2019) and monthly climatological aerosol and
 211 water vapor information. For each day and grid box the length of the period with $DNI_{ctr} \geq 120 W/m^2$ and $SZA > 2.5^\circ$ is
 212 determined and considered as the theoretically possible daylength (Figure 7).

213 W_i indicates the weighting of sunny slots depending on the number of surrounding cloudy and sunny grid points, which is
 214 discussed in more detail in Kothe et al., 2017, and remained unchanged to SARAH-2.1. The number of daylight slots
 215 ($\#\text{daylight_slots}$) describes the maximum number of Meteosat observations (slots) per grid point and per day during daylight
 216 as derived from clear sky estimations of DNI. Daily SDU is calculated only if at least 25 % of the possible daylight slots are
 217 available.

218



Clear sky daylength [h] in June



219

220 **Figure 7: Example clear sky daylength [h] based on $\text{DNI} \geq 120 \text{ W/m}^2$ for the 1th of June.**

221 2.5 Auxiliary data

222 For the generation of the SARA3-3 climate data record a few auxiliary data have been used within HelSnow and for the clear-
223 sky surface solar radiation calculations. Details are covered in the following sections.

224 2.5.1 Snow cover and sea ice thickness

225 To reduce the number of mis-classified snow-covered surfaces in the HelSnow approach, in particular in the presence of fog,
226 snow-covered surfaces are only considered in the satellite retrieval if snow is present also in global model simulations from
227 ECMWF, which use a wide range of satellite data as well as temperature information from the model simulations to determine
228 the snow-coverage of the surface.

229 Here, snow cover and sea ice data are combined and used to correct for erroneous daily snow information derived from
230 HelSnow. The global data are remapped to the spatial grid of the SARA3-3 data record. For the CDR time period of the
231 SARA3-3 data record (i.e., 1983-2020) daily 12 UTC data from ERA5-Land (snow coverage) and ERA5 (sea ice cover) (C3S,
232 2017) are used. Snow and sea ice are considered in case its coverage is higher than 50% for a certain pixel. For the period after
233 2021 (ICDR processing) the corresponding parameters are taken from the ECMWF IFS operational high-resolution forecast
234 model (IFS model) which deviate from the used ERA5 parameters. For the ICDR, snow depth and sea ice thickness are used
235 if its respective value is at least 5 cm for the grid box mean. This has been shown to deliver mostly equivalent snow and seas
236 ice masks to ERA5. Snow-coverage is only considered in the satellite retrieval if detected by the HelSnow approach; snow
237 information is not added from auxiliary data alone.

238 2.5.2 Water Vapor

239 The daily Total Column Water Vapor (TCWV) data from ERA5 is used for the CDR. For the ICDR (2021 onwards) the TCWV
240 data is used from the ECMWF IFS operational high-resolution forecast model. Thereby a daily mean is generated from 4 sub-
241 daily fields (i.e. 0, 6, 12 and 18 UTC). As the ERA5 data has a spatial resolution of $0.25^\circ \times 0.25^\circ$, the TCWV is topographically
242 downscaled to $0.05^\circ \times 0.05^\circ$ assuming a scale height of $\sim 1600\text{m}$ (see Bento, 2016). For the ICDR processing the TCWV from



243 the IFS model is used on the native grid with a spatial resolution of $0.1^\circ \times 0.1^\circ$. Like in the CDR, a daily mean is calculated
244 and used in the ICDR.

245 2.5.3 Ozone

246 In SARAH-3 daily mean values of the total vertically-integrated ozone column from ERA5 are used in a spatial resolution of
247 $0.25^\circ \times 0.25^\circ$. For the ICDR processing, daily mean total ozone from the IFS model with a spatial resolution of $0.1^\circ \times 0.1^\circ$ is
248 used, similar to the water vapor data, excluding the downscaling step. The data are used in Dobson Units.

249 2.5.4 Aerosols

250 An aerosol climatology of the European Centre for Medium Range Weather Forecast – MACC (Monitoring Atmospheric
251 Composition and Climate) is used in SARAH-3 (it had also been used for the generation of SARAH-1 and SARAH-2 (see
252 Träger-Chatterjee et al., 2014)). The original MACC climatology has been adjusted to account for the detection of high aerosol
253 loadings in the HelSnow retrieval based on the study of Müller et al., 2015.

254 2.5.5 Surface Albedo

255 New data of the surface albedo have been used in SARAH-3 compared to previous editions of SARAH for the estimation of
256 the clear-sky surface radiation. Here, monthly climatological surface albedo information based on MODIS and prepared by
257 Blanc et al., 2018, is used. This data is based on Bi-directional reflectance distribution function (BRDF) retrievals given by
258 MODIS satellite observations. The surface reflectance is provided at a spatial resolution of $0.05^\circ \times 0.05^\circ$ for five spectral
259 bands. The albedo values from the five spectral bands have been transferred to match the Kato-bands in the SPECMAGIC
260 clear sky radiative transfer model. This new monthly surface albedo background climatology used in SARAH-3 represents a
261 substantial improvement compared to previous editions of SARAH, which used surface albedo data based on land-use classes
262 without monthly variability at a much coarser spatial resolution (0.5°).

263 2.6 Daily and monthly mean generation

264 The retrieval of the surface solar radiation parameters and the effective cloud albedo is conducted for the whole time period
265 from 1 January 1983 with a temporal resolution of 30 min; the satellite slots of HH:00 and HH:30 are used for the MVIRI and
266 SEVIRI instruments, respectively. To ensure the temporal consistency of the data record, no additional satellite slots have been
267 used from the SEVIRI instrument, which does provide the satellite data with a temporal resolution of 15 min.

268 The daily means of the surface solar radiation data are based on the 30-minute instantaneous data, using the method by
269 Diekmann et al., 1988. The formula considers the diurnal cycle of surface solar radiation by using the daily-averaged and the
270 instantaneous clear-sky radiation:

$$271 \quad SSR_{DA} = SSR_{CLSDA} \frac{\sum_{i=1}^n SSR_i}{\sum_{i=1}^n SSR_{CLS_i}}$$

272 SSR_{DA} is the daily average of SSR. SSR_{CLSDA} is the daily mean clear-sky SSR (derived using SPECMAGIC every 15 minutes),
273 SSR_i and SSR_{CLS_i} are the satellite-derived SSR and model-simulated clear-sky SSR for the satellite slot i , respectively. The
274 criteria for generating a daily mean is that at least 25% of possible daytime pixels must be available (similar to the SDU
275 generation), otherwise the daily mean data is set to missing for that pixel. The daily averaging is the same for all surface solar
276 radiation parameters, including the spectral parameters. The advantage of this method to generate the daily means is that the
277 impact of missing instantaneous data on the daily averaging is much reduced. The effective cloud albedo is arithmetically
278 averaged to estimate the daily mean.

279 For the estimation of monthly averages from the daily averages the criteria as defined by WMO for the calculation of monthly
280 means are applied (WMO-No. 1203). These criteria imply that no monthly mean is estimated in case of more than ten daily



281 values or five or more consecutive daily values are missing. If the WMO-criteria are not met, the data will be set to missing
282 for these grid boxes, what occurred for three months for a larger part of the domain (1983-01, 1985-02, 1988-11). The monthly
283 means are calculated by arithmetic averaging of the daily averages.

284 3 Validation

285 The validation of each data record is an essential mandatory step that each CM SAF data record undergoes before its release.
286 The validation of SARAH-3 is documented in the CM SAF Validation Report available via
287 https://doi.org/10.5676/EUM_SAF_CM/SARAH/V003. Here we summarize the validation of the SARAH-3 CDR and ICDR
288 with surface reference measurements. We further compare the SARAH-3 data record with its predecessor SARAH-2.1, which
289 provides data from January 1983 until May 2023.

290 3.1 Reference data

291 In this section the reference data used for the validation is described. Surface measurement are used to assess the quality and
292 to validate the SARAH-3 data, as those usually offer the best data quality and can serve as reference.

293 3.1.1 Baseline Surface Radiation Network (BSRN)

294 The Baseline Surface Radiation Network (BSRN) is a widely used, high-quality network for surface radiation measurements
295 (Driemel et al., 2018, <https://bsrn.awi.de/>) maintained by the Alfred-Wegener-Institute (Helmholtz-Zentrum für Polar- und
296 Meeresforschung) in Bremerhaven, Germany. The stations are globally distributed, but their overall number is quite small (51
297 active stations at the end of 2023). The BSRN data include global, direct and direct normal solar radiation data, at most stations
298 with a temporal resolution of 1 minute and are collected with standardized high-quality measurement devices. For the
299 validation of the SARAH data records those 1-minute data are averaged to daily and monthly means using the methods as
300 recommended by Roesch et al., 2011. The BSRN archive provides data since 1994 from, in total, 76 stations, however, with a
301 changing availability of stations over time. BSRN data are used to assess the accuracy of the SARAH-3 data record; for
302 analyzing the temporal stability of a data record their usability is limited due to the comparable short duration of the time
303 series. Table 2 contains the BSRN stations used here for the validation of SARAH-3 (see section 3.3).

Station	Short name	Latitude [°]	Longitude [°]	Altitude [m]
Lerwick	ler	60.13	-1.18	84
Toravere	tor	58.25	26.46	70
Lindenberg	lin	52.21	14.12	125
Cabauw	cab	51.97	4.93	0
Camborne	cam	50.22	-5.32	88
Palaiseu Cedex	pal	48.71	2.21	156
Budapest-Lorinc	bud	47.43	19.18	139
Payerne	pay	46.82	6.94	491
Carpentras	car	44.08	5.06	100
Cener	cnr	42.82	-1.60	471
Sede Boquer	sbo	30.91	34.78	500
Solar Village	sov	24.91	46.41	650
Tamanrasset	tam	22.79	5.53	1385
Reunion Island	run	-20.90	55.48	116
Gobabeb	gob	-23.56	15.04	407
Florinopolis	flo	-27.53	-48.52	11



De Aar	daa	-30.67	24.00	1287
--------	-----	--------	-------	------

304 **Table 2: List of BSRN stations used in the validation.**

305 **3.1.2 Global Energy Balance Archive (GEBA)**

306 The Global Energy Balance Archive (GEBA) is a collection of global monthly surface irradiance data (Wild et al., 2017;
 307 <https://geba.ethz.ch/>). GEBA includes data from several hundred stations; many of those provide time series for more than 30
 308 years. The quality of the data in the GEBA archive depends on the data provider; no general quality standards for the
 309 measurements are required and no general quality control of the data is applied (as it is done as part of BSRN). To ensure the
 310 high data quality of the reference data used here, a careful selection of data from stations from the GEBA archive has been
 311 made. The criteria of this selection include a high data availability for the study period, a high spatial representativity of the
 312 station location, and a temporally homogeneous data record. The latter was determined by applying homogeneity tests using
 313 independent gridded data records as reference; these data have also been used to identify outliers in the monthly surface data,
 314 which have been removed from the analysis. The final set of 24 stations, which are used for the stability assessment of SARAH-
 315 3, are presented in Table 3.

316

Station	Latitude [°]	Longitude [°]	Altitude [m]
Ajaccio	41.917	8.8	4
Belsk	51.833	20.783	180
Bratislava	48.167	17.1	289
Braunschweig	52.3	10.45	81
Churanov	49.067	13.617	1122
Clermont-Ferrand	45.783	3.167	332
Dijon	47.267	5.083	222
Graz	46.983	15.45	342
Hradec Kralove	50.25	15.85	241
Hohenpeissenberg	47.8	11.017	990
Karlstad	59.367	13.467	46
Kolobrzeg	54.183	15.583	16
Kucharovice	48.883	16.083	334
Limoges	45.817	1.283	282
Marignane	43.433	5.217	4
Moscow University	55.7	37.5	192
Perpignan	42.733	2.867	43
Praha (Prag-Karlov)	50.067	14.433	262
Salzburg-Freisal	47.80	13.05	420
Strassburg	48.55	7.633	153
Vaexjoe-Kronoberg	56.933	14.733	182
Visby - Aerolog. Station	57.667	18.35	51
Warszawa	50.667	20.983	130
Wuerzburg	49.767	9.967	275

317 **Table 3: GEBA stations used for the validation of SARAH-3, including location longitude, latitude and elevation.**



318 **3.1.3 CLIMAT – monthly sunshine duration data**

319 CLIMAT is a set of monthly meteorological measurements shared and distributed from Meteorological Services worldwide.
320 CLIMAT data are collected and distributed by the Deutscher Wetterdienst (DWD) via the DWD Climate Data Center (CDC,
321 https://opendata.dwd.de/climate_environment/CDC/). CLIMAT includes the sunshine duration as a standard meteorological
322 parameter, which is used here for the validation of the SARA3-3 SDU data record.

323 **3.1.4 ECA&D – daily sunshine duration data**

324 The ‘European Climate Assessment and Data’ (ECA&D, <https://www.ecad.eu/>) provides station-based data of several
325 meteorological parameters at a daily resolution, including sunshine duration, for Europe (Klein Tank et al., 2002; van den
326 Besselaar et al., 2015). Here we use daily sunshine duration data from the ‘pre-defined subset’ as provided by ECA&D; non-
327 blended time series are used, i.e., the data from all individual stations are used and time series have not been merged in case
328 of station relocation / closure. As for the GEBA archive, the data quality of the data from the ECA&D data depends on the
329 data provider, no specific quality standards are applied. Also, the instruments to measure the sunshine duration are different
330 between the available time series, in particular, for those from different data providers.

331 **3.1.5 German meteorological stations**

332 The German Meteorological Service (Deutscher Wetterdienst, DWD) provides high quality observational data via its Climate
333 Data Center (CDC, www.dwd.de/cdc), mainly for Germany. Here we use daily sunshine duration and snow height data from
334 a large number of stations throughout Germany for specific validation purposes – in particular for evaluating the data quality
335 of the satellite data in case of snow cover (Section 3.2).

336 **3.2 Validation of HelSnow**

337 The newly developed HelSnow-algorithm aims to detect snow-covered surfaces and improves the ability of the algorithm to
338 distinguish between cloud- and snow-coverage in the visible-channel satellite data. This is especially relevant for clear-sky
339 situations, when previous editions of the SARA3 data record underestimated the surface solar radiation in the case of snow-
340 covered surfaces.

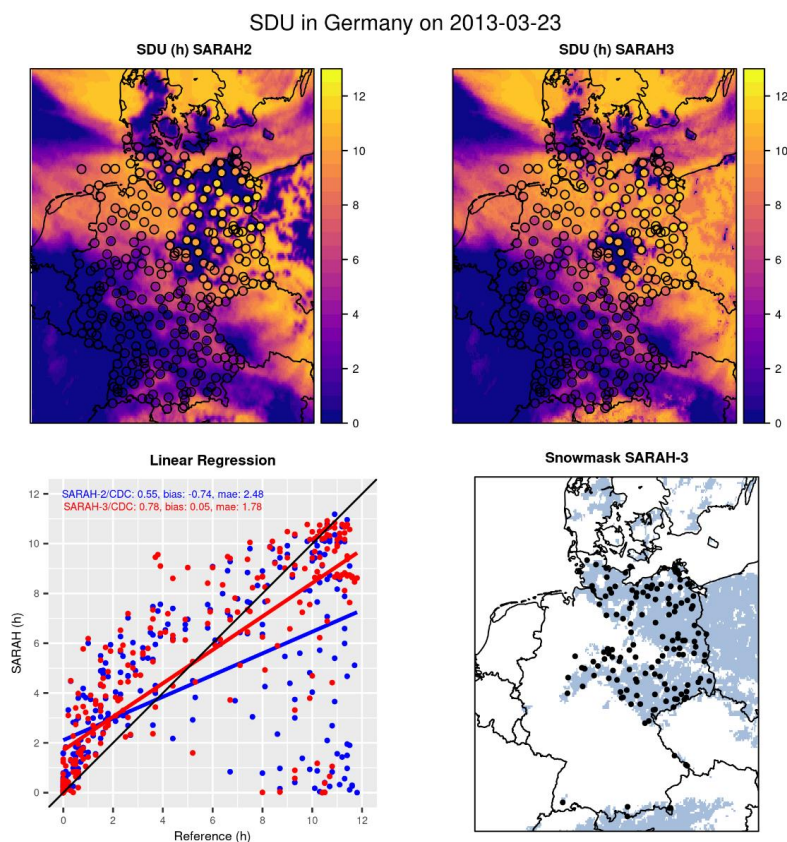
341 Figure 8 shows the case for 23 March 2013, when snow cover and clear-sky conditions occurred in Germany and neighboring
342 regions. The figure shows the improvement of the quality of the sunshine duration data from SARA3-3 compared to SARA3-
343 2.1 (compare Figure 8, top row). In particular in the north eastern part of Germany (where clear-sky prevails) the SARA3-3
344 sunshine duration compares much better to the surface reference data than the SARA3-2.1 data. In this area the snow-covered
345 surfaces were well detected by the HelSnow-algorithm (Figure 8, bottom right). The grey area (snow detected by HelSnow)
346 agrees to the snow observations from stations (black dots). The data quality improvement is also shown by the scatter plot
347 (Figure 8, bottom left): The SARA3-3 SDU (red dots) aligns much better with the 1-to-1 line than the SARA3-2.1 SDU (blue
348 dots); the mean absolute deviation between SARA3 data and the surface measurements drop from about 2.5 h (SARA3-2.1)
349 to about 1.8 h (SARA3-3).

350 A similar improvement in the data quality of the SARA3-3 surface irradiance data records is documented in Figure 9 for the
351 springtime climatological distribution of surface irradiance in the European Alpine region. Figure 9 shows a comparison of
352 surface irradiance climatologies of March derived from the SARA3-3 and the SARA3-2.1 climate data records compared to
353 surface reference observations in the European Alpine region extracted from the GEBA. Overall, in the considered regions
354 SARA3-3 shows higher climatological surface irradiance levels compared to SARA3-2.1, which agrees much better to the
355 levels derived from the surface reference measurements.

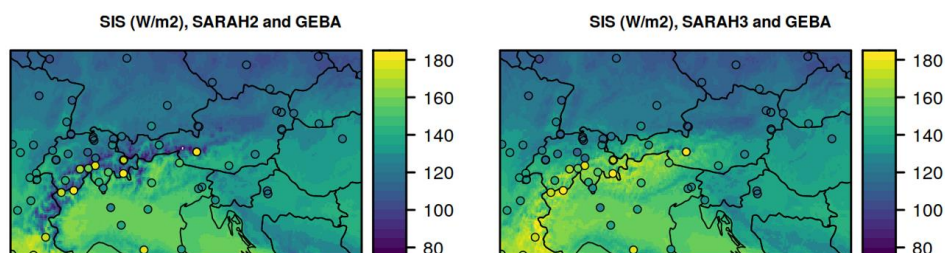
356 The ability of the HelSnow-algorithm to detect snow-covered surfaces can be determined by comparison with surface
357 observations of snow height / coverage. Here we use data of snow height for Germany from the DWD network, which is



358 available for the temporal coverage of the satellite data record. Figure 10 shows the results of the comparison between the
359 satellite-derived snow mask and the surface measurements for all winter seasons from 1983 to 2019 using the categorical ACC
360 score, defined as the number of correct detections (snow and no-snow) over all cases, and the mean number of days with snow
361 for each season. Overall, the high levels of the ACC-score (median value for almost all years > 0.8) indicate a good quality of
362 the snow mask. A reduced ACC score is correlated with a larger number of days with snow, indicating an underestimation of
363 snow detection by HelSnow. It is worth noting that this evaluation includes situations with snow coverage under cloudy sky;
364 in such situations a snow detection is not possible from the satellite data in the visible channel and the information on snow
365 coverage is estimated from the previous day. The surface solar radiation retrieval, however, is not using the snow information
366 on cloudy days (see section 2.1.4).
367 The quality of the internal snow-mask slightly improves over time, but is rather stable since the early 1990s. (Figure 10). The
368 reason for the reduced quality of the snow detection in the early years of the SARA3 data record is the reduced quality of
369 the satellite input data from the early METEOSAT satellites (less stable, many missing data), which negatively affects the
370 snow detection capability, and the high number of days with snow coverage, which also influences the accuracy of the
371 HelSnow-algorithm. This reduced snow detection quality results in an underestimation of snow and in a more frequent
372 misclassification of snow- as cloud-coverage, which subsequently might lead to a more frequent underestimation of surface
373 solar radiation in the early years of the SARA3 data record.

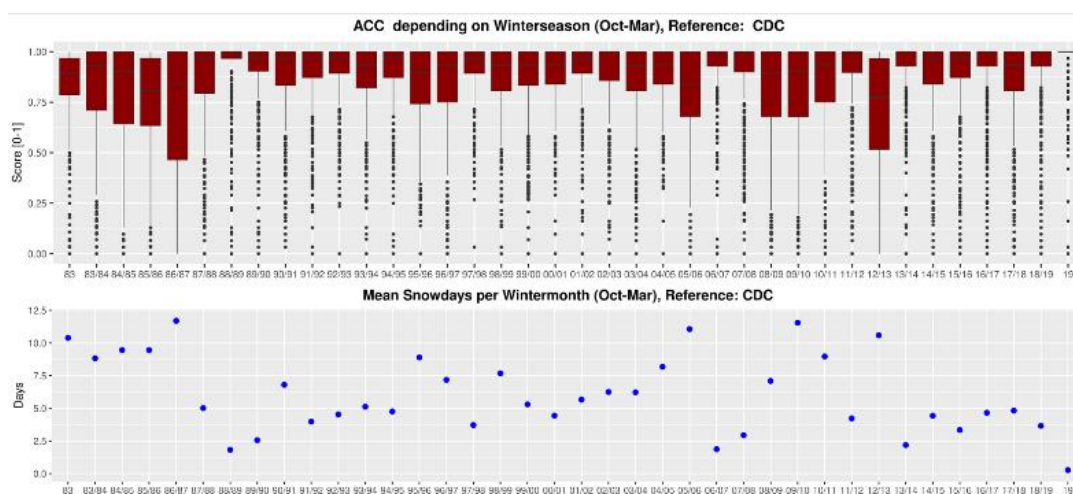


374
375 **Figure 8:** Comparison of sunshine duration from SARAH-3 (top right) and its predecessor SARAH-2.1 (top left) for a snow case in
376 Germany at 2013-03-23 and comparison to station observations of sunshine duration (dots with same colorbar). The map at bottom
377 right shows the snow cover as detected by HelSnow (grey pixels) and the station data with snow observations (black dots) as overlay.
378 The scatterplot (bottom left) shows SARAH-3 SDU (red dots) and SARAH-2.1 SDU (blue dots) vs the station observations of SDU
379 (bottom right). Included are the linear regressions and its functions and the 1:1 line in black.



380
381 **Figure 9:** Validation of surface irradiance (SIS) climatology of SARH-2.1 (left) and SARAH-3 (right) for March together with station
382 observations from GEBA for the alpine region.

383

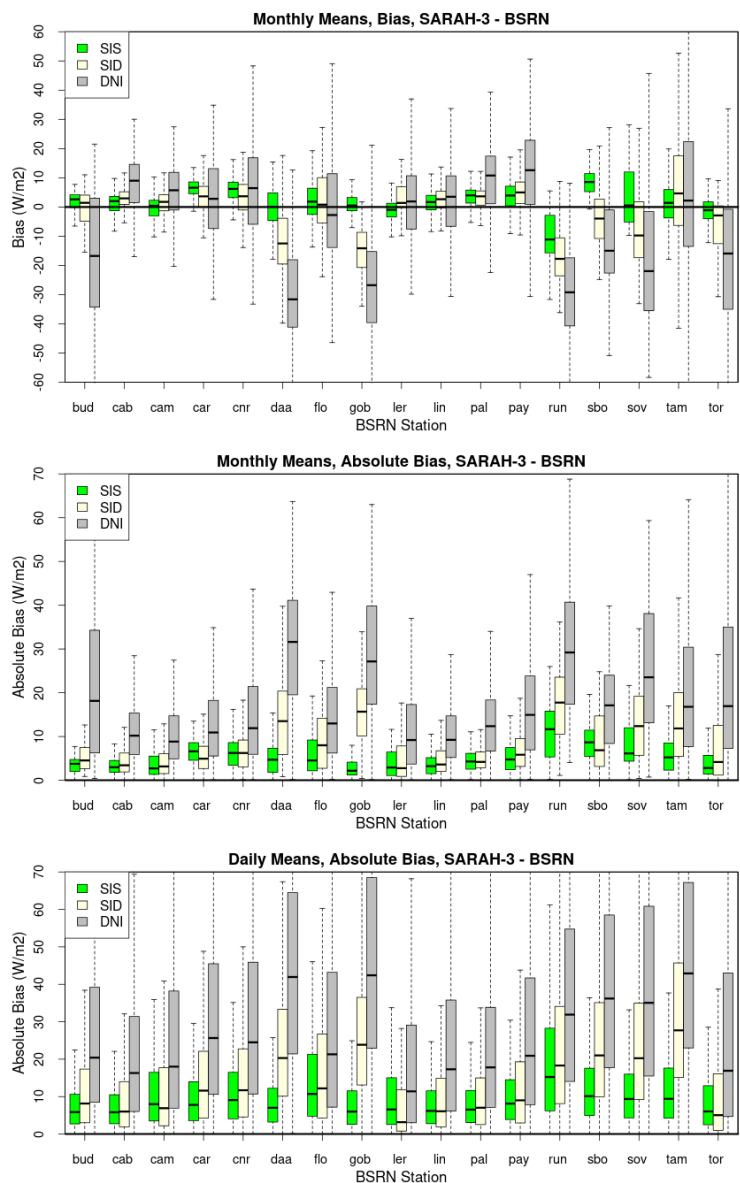


384
385 **Figure 10:** Time series (1983-2019) of the ACC-Score to validate the snow mask derived by HelSnow with reference to German CDC
386 snow observations. The ACC-score is the measure of the correct (snow or no snow) estimates over all estimates.

387 3.3 Accuracy validation

388 3.3.1 Validation with BSRN data

389 Data from the Baseline Surface Radiation Network (BSRN) are the most important reference data source for the validation of
390 surface radiation data in the CM SAF. The main validation results of the SARAH-3 surface irradiance (SIS) and direct
391 irradiance data records (SID and DNI) using BSRN data for the time period 1994-2020 are shown in Figure 11 for monthly
392 and daily averages. For the comparison, data from the SARAH-3 grid box that is closest to the corresponding BSRN station is
393 used.



394

395 **Figure 11: Validation results of the SARAH-3 parameters surface irradiance (SIS, green), surface direct irradiance (SID, yellow)**
 396 **and direct normal irradiance (DNI, grey) with individual BSRN stations. Shown are boxplots for the monthly mean bias (top), the**
 397 **monthly absolute bias (center) and the daily absolute bias (bottom). All data are in W/m^2 . The short names of the BSRN stations are**
 398 **listed in Table 2.**

399 Figure 11 shows that the bias and the Mean Absolute Deviation (MAD) are lower for the surface irradiance (SIS), and higher
 400 for the direct irradiance parameters SID and DNI. For the surface irradiance the bias is rather small for most locations, only
 401 for the BSRN stations of Reunion Island (negative bias) and Sede Boquer (positive bias) the bias is somehow conspicuous
 402 larger than for other locations; the biases are larger, in general, for the direct irradiance parameters (SID and DNI). Concerning
 403 the mean absolute deviations (MAD) the situation is comparable (see Figure 11 middle and bottom): The MAD for the direct
 404 irradiance parameters are larger than for the surface irradiance. The overall validation results of SARAH-3 vs. BSRN stations
 405 for monthly and daily data are summarized in Table 4.

406



Parameter	SIS		SID		DNI	
	mm	dm	mm	dm	mm	dm
temp.res.						
Bias [W/m^2]	2.1	2.1	0.68	0.65	-1.3	0.0
MAD [W/m^2]	5.3	10.8	7.9	16.1	16.8	31.1
Anomaly Cor.	0.94	0.96	0.91	0.93	0.90	0.93

407 **Table 4: Summary of validation results of surface irradiance (SIS), surface direct irradiance (SID) and direct normal irradiance**
 408 **(DNI) vs. BSRN stations, for monthly (mm), daily (dm) SARAH-3 data. Shown is the bias, the mean absolute deviation (MAD), and**
 409 **the anomaly correlation (Anomaly Cor.).**

410 Table 4 shows that the mean bias for all parameters is small with $\pm 2 \text{ W/m}^2$. The mean absolute biases (MAD) are lowest for
 411 the surface irradiance (SIS) and higher for the direct solar radiation parameters SID and DNI. In general, the monthly means
 412 have lower MAD values than the daily means, as daily deviation partly average out over the course of a month. For the monthly
 413 means the MAD for SIS is only about 5 W/m^2 . The correlations of the anomalies between the SARAH-3 data records and the
 414 BSRN reference data reach and exceed 0.9 for all parameters, documenting the high quality of the SARAH-3 to identify and
 415 to quantify anomalies in the surface solar radiation, which is an important application for climate data records as well.

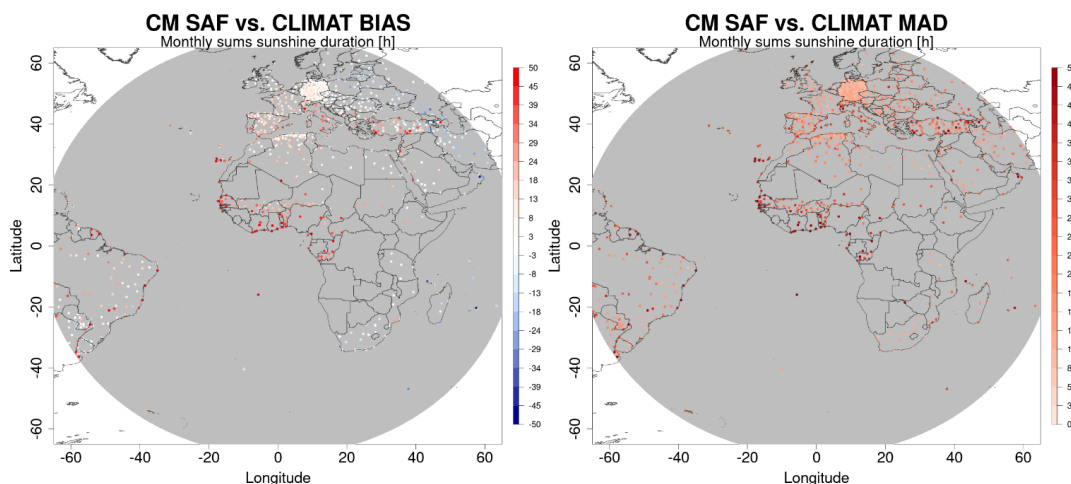
416 3.3.2 Validation of Sunshine Duration

417 Sunshine Duration is a highly relevant climate variable with a long history of surface measurements. It is measured for more
 418 than 150 years and is of high relevance for life. There are many sunshine duration measurements available for validation
 419 purposes. For the SARAH-3 SDU validation we are making use of the monthly CLIMAT data and the daily SDU data from
 420 the ECA&D. The validation results are summarized in Table 5. For the monthly sums, the SDU bias is about 10 hours on
 421 average and about 0.2 hour (or about 12 minutes) for the daily sums. Due to its higher variability concerning day to day
 422 variations, the anomaly correlation of SARAH-3 and the stations is higher for daily sums than for monthly sums. The mean
 423 absolute deviations are only about 1 hour for the daily sums of sunshine duration.

	Bias	MAD	Anom.Cor.	Number Obs.
SDU monthly sum	9.5 h	20 h	0.84	335.705
SDU daily sum	0.2 h	1 h	0.93	10.163.793

424 **Table 5: Summary of the validation of the monthly and daily SARAH-3 SDU with reference to monthly CLIMAT and daily ECA&D**
 425 **sunshine duration data.**

426 Figure 12 shows maps of the mean bias and mean absolute deviations (MAD) per station of the monthly SARAH-3 SDU data
 427 minus the CLIMAT station data. The figure shows that the bias and the MAD are small for most stations, but larger for the
 428 tropical and subtropical stations of Africa. For parts of south eastern Europe, the deviations are larger as well. For the majority
 429 of African stations SARAH-3 has a positive bias concerning monthly sums of SDU, reaching values of more than 30 hours.
 430



431

432 **Figure 12: Map of biases (left) and mean absolute deviations (MAD) (right) for monthly sunshine duration from SARAH-3 minus**
433 **CLIMAT stations.**

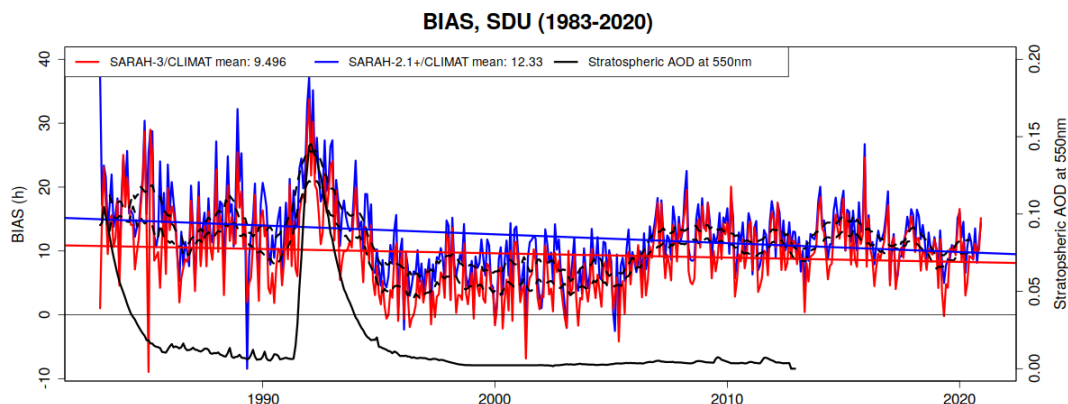
434

435 3.4 Stability validation

436 3.4.1 Sunshine duration validation with CLIMAT

437 The availability of the long times series of sunshine duration in the CLIMAT data archive allows the analysis of the temporal
438 stability of the SARAH-3 sunshine duration data. The temporal evolution of the bias between the SARAH-3 and the reference
439 data reveals fluctuations and deviations, in particular during the early years of the data record (Figure 13). In the early 1990s
440 there is a period with more positive deviations by SARAH-3, which might be related to the volcanic eruption of Mount
441 Pinatubo on the Philippines in 1991 (Vernier et al., 2011).

442 The increase of the atmospheric optical depth due to additional aerosols, e.g. by volcanic eruptions, is not directly accounted
443 for in the SARAH retrieval and, hence, might result in an overestimation of SDU in that particular period. The slight and
444 gradual increase of the bias in the mid-2000s is not associated with volcanic activity and requires further analysis. The data
445 quality of SARAH-3 is improved, compared to SARAH-2.1, in terms of the mean bias (~9.5 h vs ~12.3 h) by more than 20%
446 as well as the stability of SARAH-3 as documented by the linear regression lines in Figure 13. Overall there is a slight negative
447 trend in the bias vs the CLIMAT SDU measurements.



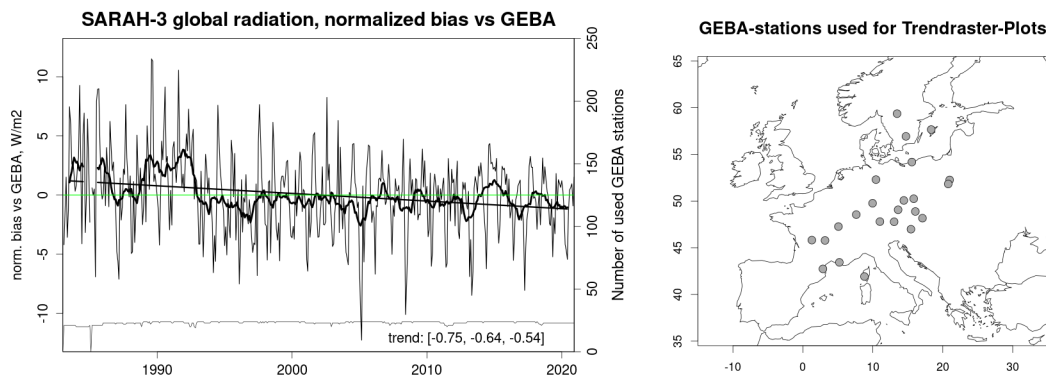
448

449 **Figure 13:** Bias time series of the monthly sunshine duration (SDU) in hours of SARAH-3 vs CLIMAT (red) and SARAH-2.1
450 vs CLIMAT (blue) for the time period 1983-2020. Additionally, the linear regression lines for both bias time series and the 12-month
451 running means of both bias time series are shown. The black line shows the stratospheric aerosol optical depth (AOD) at 550nm
452 provided by National Aeronautics and Space Administration (NASA) - Goddard Institute for Space Studies (see
453 <https://data.giss.nasa.gov/modelforce/strataer/#References> for details of the used aerosol data). The mean bias of the SARAH-3 SDU
454 and SARAH-2.1 SDU vs CLIMAT station observations is also provided at the top of the figure.

455 3.4.2 Surface irradiance validation with GEBA

456 The monthly surface irradiance data from the GEBA archive is used to assess the long-term stability of the SARAH-3 surface
457 solar radiation climate data record in Europe. Figure 14 (left) shows the time series of the normalized bias between the data
458 from the 24 GEBA stations and the SARAH-3 surface irradiance data record. The numbers at the bottom right of Figure 14
459 (left) represent the slope of the linear regression line (number in the middle) and its 95% confidence interval (ci), indicating
460 the linear trend of the time series. The 95%-ci defines the range of values, in which the true slope of the linear regression is
461 located with a probability of 95%. The linear trend of the bias based on the 12-monthly running mean time series is -0.64
462 $\text{W/m}^2/\text{decade}$, which in turn means that a potential trend in the data from the GEBA stations is underestimated by SARAH-3
463 by about $0.6 \text{ W/m}^2/\text{decade}$. The number of stations used for this analysis is rather stable over time due to the used set of selected
464 stations from GEBA (see Section 3.1.2). The number of stations drops to almost zero in February 1985 due to missing data in
465 the SARAH-3 data record for that month as result of the application of the rather strict criteria for the monthly mean generation
466 based on WMO (see Section 2.6).

467 Figure 14 shows that there is a positive anomaly in the SARAH-3 surface irradiance data record in the early 1990s, which
468 might be related to the Pinatubo volcanic eruption in June 1991. This eruption emitted huge amounts of sulphate into the
469 stratosphere, resulting in the formation of sulphate aerosol, which caused a dimming of the solar radiation in the years
470 afterwards. This dimming by the volcanic aerosols is not accounted for in the SARAH-3 data record, which might cause an
471 overestimation of the surface solar radiation by SARAH-3. A similar behavior in the temporal evolution of the bias has been
472 overserved for the sunshine duration in the early 1990s (see Section 3.4.1). On the other hands, the increase in the surface
473 irradiance bias starts already in 1989, i.e., prior to the Pinatubo eruption, and other factors are likely to contribute to this
474 increase. The decrease of the tropospheric aerosol optical depth due to the reduction of air pollution after 1989 in Europe might
475 also have contributed to the overestimation of surface irradiance by SARAH-3 in this time period.



476

477

478

479

480

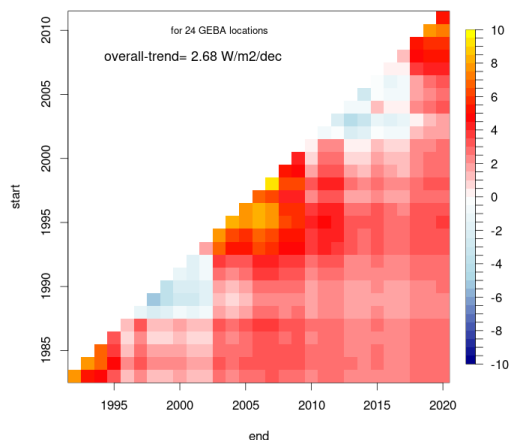
481

482

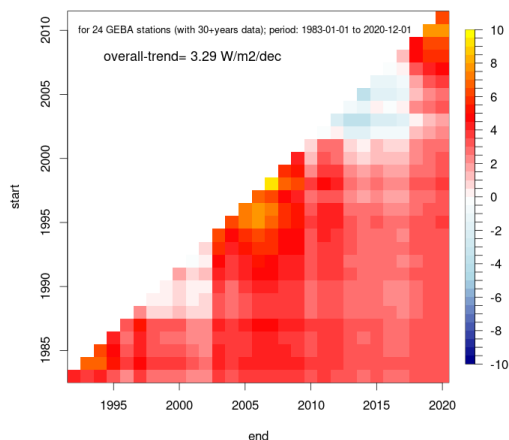
483

Figure 14: Left side: Time series of the monthly and 12-monthly rolling means of normalized bias (meaning the overall bias of 3 W/m^2 is subtracted) between the SARAH-3 surface irradiance data record and the GEBA station data for the time period 1983-2020 (black line) including the linear trend line (black) based on the 12-month rolling means. The green line represents the zero-trend line. The grey line (at the lower part) shows the time series of the number of stations used. Additionally, the trend based on the linear regression and its confidence interval are printed (W/m^2 , lower right). Thereby the first number is the lower end of the confidence interval, the 2nd number is the trend and the 3rd number is the upper end of the confidence interval. Right side: Map of the GEBA stations used.

SARAH-3 SIS Trendrafter-Plot [$\text{W/m}^2/\text{decade}$], Europe, 1983-2020



GEBA SIS Trendrafter-Plot [$\text{W/m}^2/\text{decade}$], Europe, 1983-2020



484

485

486

487

Figure 15: “Trendrafter-Plot” of the SARAH-3 (left) and GEBA (right) surface irradiance for the 24 used GEBA stations. Y-axis denote start of trends and x-axis denote end of trends. Trends shown range from 10 years to 38 years (the maximum length of trend, shown in the lower right part of the Trendrafter).

488

489

490

491

492

493

494

495

496

497

The “running trend” analysis (visualized by so-called “Trendrafter”-plots) enables to analyze and to compare variability and trends between two data sets. Figure 15 shows the linear trends over different time period of 10 years and longer; the y-axis denotes the start of a trend estimate and the x-axis denotes the end of a trend estimate. The diagonal shows the shortest (10 year) trends. Figure 15 shows that the temporal pattern of trends as given by SARAH-3 (Figure 15 left) and GEBA (Figure 15 right) are very similar for the average of the used stations. The overall long-term trends of surface irradiance for the period 1983-2020 are also provided in the figure. The trend in SARAH-3 is about $+2.7 \text{ W/m}^2/\text{decade}$ and the corresponding trend by GEBA is about $+3.3 \text{ W/m}^2/\text{decade}$. The difference between the trends is about $0.6 \text{ W/m}^2/\text{decade}$ in line with the trend in the bias between both data sets (Figure 14). There is a substantial variability in the decadal trend estimate, which is well represented by the SARAH-3 SIS data record (Figure 15). This variability highlights the high relevance of the start- and the end-year for trend analysis, as can also be seen by patterns (vertical and horizontal lines) caused by the end years 2003 and 2013, that



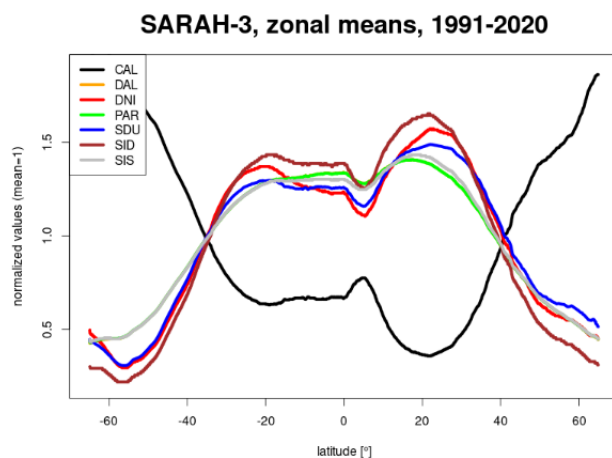
498 experience strong positive and negative anomalies of surface irradiance, respectively. In other words, trends ending (starting)
499 in 2003 tend to be exceptionally positive (negative).

500 4 Applications

501 In this section we will demonstrate some applications of the SARA3 climate data record.

502 4.1 Climatology

503 A basic application of a climate data record is the calculation of a climatology by averaging the monthly means for a certain
504 time period. SARA3 covers the current WMO climate normal period from 1991 to 2020; the climatology of surface
505 irradiance for the full SARA3 domain is shown in Figure 1. It shows the typical pattern of maximum surface solar radiation
506 in the subtropics, in particular in the northern hemisphere and minimum surface solar radiation in the high latitudes. In the
507 tropics there is a local minimum due to the frequent occurrence of clouds in the Inter Tropical Convergence Zone (ITCZ).
508 Figure 16 shows the zonal means of all SARA3 parameters for the full domain. The meridional variability of the Effective
509 Cloud Albedo (CAL) is opposite to the surface solar radiation parameters, which follows the relation of CAL to surface solar
510 radiation, as described in Section 2.3.



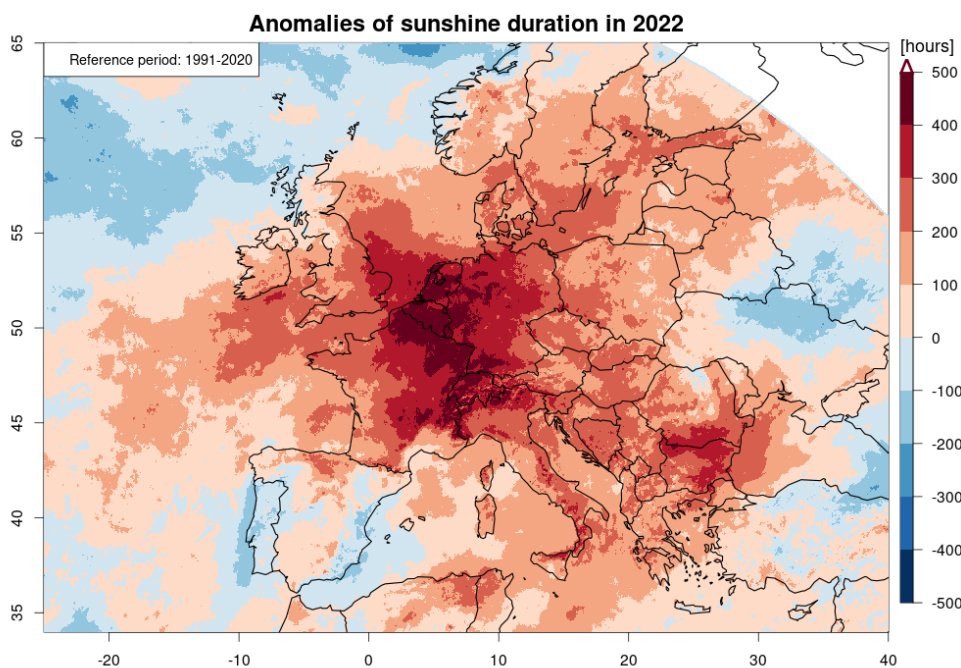
511
512 **Figure 16: Zonal means of all SARAH-3 parameters for the full SARAH-3 domain. The parameters are normalized with their**
513 **respective mean value.**

514 All surface solar radiation parameters behave similar concerning the zonal means, however there are also some differences.
515 The normalised surface irradiance (SIS) is substantially larger than the normalised direct radiation parameters (SID and DNI)
516 at latitudes of $\sim 50^\circ\text{S}$, where the clear-sky situations are relatively seldom. On the other hand, the situation is the opposite for
517 the subtropics, where cloudy days are rare. There, the normalized values for the direct radiation parameters are higher than for
518 the global radiation (i.e. surface irradiance). A local minimum in all surface solar radiation parameters is visible in the inner
519 tropics ($\sim 5^\circ\text{N}$), where clouds are relatively frequent due the frequent occurrence of convection in the ITCZ. The range of the
520 zonal averages is highest for the normalised direct surface irradiance (SID), while the normalised surface irradiance has the
521 lowest meridional variability. The high cloud coverage south of 40°S results in the low values for the direct radiation
522 parameters (SID, DNI) and the sunshine duration, in particular when compared to the surface irradiance (SIS), which also
523 includes the diffuse radiation and, subsequently, is impacted slightly less by cloud coverage. The minimum / maximum of the
524 effective cloud albedo / the surface solar radiation parameters at about 20°N corresponds to the large desert area in northern
525 Africa, which has no correspondence in the southern hemisphere due to the larger oceanic contribution.



526 **4.2 Climate Monitoring**

527 SARAH-3 is accompanied by an Interim Climate Data Record (ICDR) that consistently extends the Climate Data Record
528 (CDR) in time. The CDR and ICDR-combination is a powerful tool for climate monitoring applications. The committed
529 timeliness of the SARAH-3 ICDR is five days, but usually the SARAH-3 ICDR comes with a timeliness of only two days.
530 Figure 17 shows the spatial distribution of the annual anomaly of sunshine duration for 2022 relative to the climate normal
531 period (1991-2020). The map shows that 2022 was much sunnier than normal (up to +500 hours of sunshine) in parts of Central
532 Europe (Germany, BeNeLux, France); parts of the Iberian Peninsula were less sunny than usual in 2022. The SARAH-3
533 CDR+ICDR combination is used, for example, by the Copernicus European State of the Climate reports (ESOTC; C3S, 2023)
534 and by the WMO Regional Climate Center (RCC) for the European area ([https://rcccm.dwd.de/DWD-](https://rcccm.dwd.de/DWD-RCCCM/EN/home/home_node.html)
535 [RCCCM/EN/home/home_node.html](https://rcccm.dwd.de/DWD-RCCCM/EN/home/home_node.html)).



536
537 **Figure 17: Anomaly of the SARAH-3 sunshine duration [hours] for 2022, with reference to the climate normal period (1991-2020).**

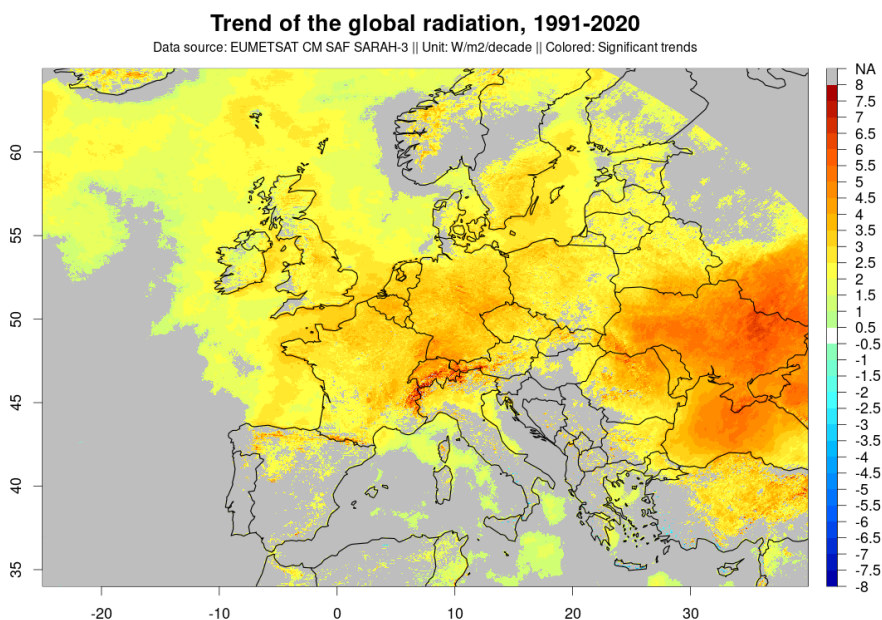
538 **4.3 Climate Variability and Trends**

539 Using a data record for assessing climate variability and trends requires a high level of data quality. Especially the temporal
540 stability of a data record is crucial for such analyses. Based on the experiences with the previous editions of SARAH (e.g.,
541 Pfeifroth et al., 2018) and based on the SARAH-3 validation results, we conclude that it is feasible to calculate trends with a
542 reasonable confidence, in particular for Europe after about 1990 (see Section 3.4.2). However, it should be mentioned here
543 that further analyses and validation are required to assess the stability of the SARAH-3 data record for other regions and
544 periods.

545 Figure 18 shows the trends of the SARAH-3 surface irradiance (also called global radiation) for the climate normal period
546 (1991-2020) focusing on Europe. The climate normal period was chosen in order to foster comparability; further, the 1980s
547 with reduced data quality in satellite and station data are avoided when using the WMO climate normal period. Pixels are only
548 colored in case the trend is statistically significant. The trend and the significance values are derived using the “trend”-function
549 from the CM SAF R Toolbox (Kothe et al., 2019). A trend for pixel is considered to be significantly positive (negative) if the



550 95% confidence interval of the slope of the linear trend (see section 3.4.2 for details) is completely positive (negative). For
551 Europe, there are significant positive trends of surface irradiance given by SARAH-3 over the period 1991-2020. Strongest
552 positive trends are located in Central and Eastern Europe with trends in the range of 2-5 W/m²/decade. Also, parts of the
553 European Alps stand out with large significantly positive trends of up to 7 W/m²/decade, where the snow detection by the
554 HelSnow-algorithm might impact the estimated trend resulting in an overestimation of the trend (see also Section 3.2). There
555 are almost no significant negative trends of surface irradiance in Europe for the period between 1991 and 2020.



556
557 **Figure 18: Trend of the SARAH-3 global radiation in Europe for the climate normal period (1991-2020). Pixels are only colored in**
558 **case of the trend being statistically significant.**

559 5 Data availability

560 The data record doi for SARAH-3 is https://doi.org/10.5676/EUM_SAF_CM/SARAH/V003 (Pfeifroth et al., 2023). Data and
561 associated documentation (scientific references, algorithm theoretical basis documents, validation reports, and user manuals)
562 are available through the following link: https://doi.org/10.5676/EUM_SAF_CM/SARAH/V003 (Pfeifroth et al., 2023).
563 All intellectual property rights of the CM SAF SARAH-3 products belong to EUMETSAT. The use of these products is granted
564 to every interested user, free of charge. If you wish to use these products, EUMETSAT's copyright credit must be shown by
565 displaying the words "copyright (year) EUMETSAT" on each of the products used.

566 6 Conclusions

567 SARAH-3 is the new edition of the satellite-based surface solar radiation climate data record (released in May 2023) by the
568 EUMETSAT Satellite Application Facility on Climate Monitoring. SARAH-3 provides data since 1983 (i.e., for more than 40
569 years) with a spatial resolution of 0.05° and a temporal resolution of up to 30 minutes for Europe, Africa, and parts of Southern
570 America as well as for parts of the Atlantic and the Indian Ocean. SARAH-3 includes seven parameters (see Table 1) including
571 surface irradiance, surface direct radiation parameters, sunshine duration; and the Photosynthetic Active Radiation (PAR) and
572 Daylight (DAL) that are new parameters in SARAH-3. The main improvement of SARAH-3 is the improved surface solar



573 radiation estimation in presence of snow cover, that is internally derived by the HelSnow algorithm. Further, several auxiliary
574 data are updated, incl. the surface albedo, which now has a spatial resolution comparable to the SARA3-3 data itself. The
575 SARA3-3 data record and all other data records released by the CM SAF are available free of charge via the CM SAF Web
576 User Interface (www.wui.cmsaf.eu) in NetCDF-format.

577 The algorithm used to generate SARA3-3 has been subject to continuous developments since the 1st release of a METEOSAT-
578 based surface radiation data record by the CM SAF, while the basic algorithmic approach (i.e., a Heliosat-based retrieval) has
579 been unchanged. The improved auxiliary data has also contributed to improved final data products, e.g. through the usage of
580 daily ERA5 atmospheric background fields, instead of monthly ERA-Interim data. The new snow detection by HelSnow leads
581 to improved accuracy and reduced biases, especially in case of snow cover and clear-sky conditions (see Section 0).

582 The validation (see Section 3) shows that SARA3-3 offers high quality climate data; the uncertainty of the data increases with
583 increasing temporal resolutions. The validation of the SARA3-3 direct solar radiation parameters shows higher deviations to
584 surface reference measurements than for the surface irradiance (called global radiation). For the latter, the mean absolute
585 deviations between the SARA3-3 data and surface reference measurements are about 5 W/m² and 11 W/m² for monthly and
586 daily averages, respectively. Note that these measures include the uncertainties of the surface measurements and are impacted
587 by the difficulty of comparing point measurements to grid-box averages. An important validation measure for climate data
588 records is also its ability to detect and quantify anomalies, which is measured by the anomaly correlation. For SARA3-3 the
589 corresponding correlation coefficients are between 0.84 and 0.98, documenting the ability to use the SARA3-3 data for climate
590 monitoring applications (see Section 4.2).

591 The stability of SARA3-3 has been found to be high and further improved relative to its predecessor. The comparison with
592 long-term surface reference measurements in Europe from GEBA revealed that there is a small negative trend in the time series
593 of the bias between SARA3-3 and surface reference data of about -0.6 W/m²/decade for surface irradiance for the period 1983-
594 2020. Further, trends in the European Alps are likely overestimated by SARA3-3 when considering the full time series of the
595 data record (1983 onwards). The reason for this trend overestimation is the reduced quality of the snow detection by HelSnow
596 for the early years of the data record. For the climate normal period of 1991-2020, and onwards, this issue is strongly reduced,
597 and hence the stability in the Alpine region is improved from the 1990s onwards. The 1991 Pinatubo volcanic eruption likely
598 led to an overestimation of the surface solar radiation and sunshine duration during that period of enhanced aerosol loadings
599 in the stratosphere.

600 In Section 4 some example applications of the SARA3-3 data record are shown. The climatology of a certain parameter gives
601 insights to the spatial distribution of the respective parameter, which is useful for many applications. For the first time the
602 current SARA3 climate data record covers the current climate normal period from 1991 to 2020. In addition, the availability
603 of instantaneous (30-minutes), daily and monthly data and of data from the ICDR, which operationally extends the data record,
604 allows a wide range of applications of the SARA3-3 climate data record, including climate monitoring, see Figure 17, and
605 climate analyses. The interpretation, however, of long-term trends should be done with care, since such trends are strongly
606 influenced by anomalies at the beginning and end of the time series considered. The validation results of SARA3-3 show that
607 the data can be used for trend analysis with reasonable confidence. The linear trend of the SARA3-3 global radiation for 1991-
608 2020 in Europe is overall positive, which is in line with surface observations (see Figure 15).

609 With its numerous surface solar radiation parameters, high quality, long time series, high spatial and temporal resolution and
610 high timeliness (~2 days), the freely available SARA3-3 data record continues to serve users in many fields of research and
611 operation. In case of questions or inquiries regarding the SARA3-3 data (or any other CM SAF data), the CM SAF User Help
612 Desk is available via contact.cmsaf@dwd.de.

613



614 **Author contribution**

615 UP prepared the original manuscript with substantial contributions from JT. JD contributed to the data validation of sunshine
616 duration. UP and JT developed and validated the surface radiation products. UP generated the data record, supported by SK
617 and supervised by JT. MS and RH provided valuable comments and recommendations for the structure of the manuscript. All
618 authors contributed to the manuscript. All authors contributed the writing or reviewing and editing.

619 **Acknowledgement**

620 The authors acknowledge the financial support of the EUMETSAT member states through the Satellite Application Facility
621 on Climate Monitoring. Further, the authors like to thank Ruben Urraca for the cooperation on the quality control and usage
622 of the GEBA surface reference measurements. Further we thank the World Radiation Monitoring Center – Baseline Surface
623 Radiation Network (BSRN) and the Global Energy Balance Archive (GEBA) for providing surface reference data. GEBA is
624 co-funded by the Federal Office of Meteorology and Climatology MeteoSwiss within the framework of GCOS Switzerland.
625 We also thank Prof. Elmar Schömer and Kai Wirtz from the Johannes Gutenberg-University of Mainz for the HelSnow
626 development.

627 **Competing interests**

628 The contact author has declared that none of the authors has any competing interests.

629 **7 References**

- 630 Kato, S., Ackerman, T., Mather, J., and Clothiaux, E.: The k-distribution method and correlated-k-approximation for short-
631 wave radiative transfer model, *J. Quant. Spectrosc. Radiat. Transf.*, 62, 109–121, 1999
- 632 Wild, M., Folini, D., Schär, C. *et al.* The global energy balance from a surface perspective. *Clim Dyn* 40, 3107–3134 (2013).
633 <https://doi.org/10.1007/s00382-012-1569-8>
- 634 Pfeifroth, U., Bojanowski, J. S., Clerbaux, N., Manara, V., Sanchez-Lorenzo, A., Trentmann, J., Walawender, J. P., and
635 Hollmann, R.: Satellite-based trends of solar radiation and cloud parameters in Europe, *Adv. Sci. Res.*, 15, 31–37,
636 <https://doi.org/10.5194/asr-15-31-2018>, 2018.
- 637 Hartmann, D. L., Ramanathan, V., Berroir, A., and Hunt, G. E.: Earth Radiation Budget data and climate research, *Rev.*
638 *Geophys.*, 24, 1944–9208, <https://doi.org/10.1029/RG024i002p00439>, 1986
- 639 Wild, M. (2016), Decadal changes in radiative fluxes at land and ocean surfaces and their relevance for global warming.
640 *WIREs Clim Change*, 7: 91-107. <https://doi.org/10.1002/wcc.372>
- 641 Ramanathan, V., Crutzen, P. J., Kiehl, J. T., & Rosenfeld, D. (2001). Aerosols, climate, and the hydrological cycle. *Science*,
642 294(5549), 2119–2124. <https://doi.org/10.1126/science.1064034>
- 643 Gautier, C., G. Diak, and S. Masse, 1980: A Simple Physical Model to Estimate Incident Solar Radiation at the Surface from
644 GOES Satellite Data. *J. Appl. Meteor. Climatol.*, 19, 1005–1012, [https://doi.org/10.1175/1520-0450\(1980\)019<1005:ASPMTE>2.0.CO;2](https://doi.org/10.1175/1520-0450(1980)019<1005:ASPMTE>2.0.CO;2).
- 645
646 Pinker, R. T., and I. Laszlo, 1992: Modeling Surface Solar Irradiance for Satellite Applications on a Global Scale. *J. Appl.*
647 *Meteor. Climatol.*, 31, 194–211, [https://doi.org/10.1175/1520-0450\(1992\)031<0194:MSSIFS>2.0.CO;2](https://doi.org/10.1175/1520-0450(1992)031<0194:MSSIFS>2.0.CO;2).
- 648 Rigollier, M.; Levefre, M.; Wald, L. The method Heliosat-2 for deriving shortwave solar radiation from satellite images. *Solar*
649 *Energy* 2004, 77, 159–169.



- 650 Vernay, C.; Pitaval, S.; Blanc, P. Review of satellite based surface solar irradiation databases for the engineering, the financing
651 and the operating of photovoltaic systems. *Energy Procedia* 2014, 57, 1383–1391.
- 652 Möser, W.; Raschke, E. Incident solar radiation over Europe estimated from METEOSAT data. *J. Clim. Appl. Meteorol.* 1984,
653 23, 166–170.
- 654 Cano, D.; Monget, J.; Albuissou, M.; Guillard, H.; Regas, N.; Wald, L. A method for the determination of the global solar
655 radiation from meteorological satellite data. *Solar Energy* 1986, 37, 31–39.
- 656 Schulz, J., Albert, P., Behr, H.-D., Caprion, D., Deneke, H., Dewitte, S., Dürr, B., Fuchs, P., Gratzki, A., Hechler, P., Hollmann,
657 R., Johnston, S., Karlsson, K.-G., Manninen, T., Müller, R., Reuter, M., Riihelä, A., Roebeling, R., Selbach, N., Tetzlaff, A.,
658 Thomas, W., Werscheck, M., Wolters, E., and Zelenka, A.: Operational climate monitoring from space: the EUMETSAT
659 Satellite Application Facility on Climate Monitoring (CM-SAF), *Atmos. Chem. Phys.*, 9, 1687–1709,
660 <https://doi.org/10.5194/acp-9-1687-2009>, 2009.
- 661 Pfeifroth, Uwe; Kothe, Steffen; Drücke, Jaqueline; Trentmann, Jörg; Schröder, Marc; Selbach, Nathalie; Hollmann, Rainer
662 (2023): Surface Radiation Data Set - Heliosat (SARAH) - Edition 3, Satellite Application Facility on Climate Monitoring,
663 DOI:10.5676/EUM_SAF_CM/SARAH/V003, https://doi.org/10.5676/EUM_SAF_CM/SARAH/V003.
- 664 Posselt, Rebekka; Müller, Richard; Stöckli, Reto; Trentmann, Jörg (2011): CM SAF Surface Radiation MVIRI Data Set 1.0 -
665 Monthly Means / Daily Means / Hourly Means, Satellite Application Facility on Climate Monitoring,
666 DOI:10.5676/EUM_SAF_CM/RAD_MVIRI/V001, https://doi.org/10.5676/EUM_SAF_CM/RAD_MVIRI/V001
- 667 Copernicus Climate Change Service (C3S), 2023: European State of the Climate 2022, Full report:
668 climate.copernicus.eu/ESOTC/2022
- 669 Kothe, S.; Pfeifroth, U.; Cremer, R.; Trentmann, J.; Hollmann, R. A Satellite-Based Sunshine Duration Climate Data Record
670 for Europe and Africa. *Remote Sens.* **2017**, 9, 42
- 671 Drücke, J.; Borsche, M.; James P.; Kaspar, F.; Pfeifroth, U.; Ahrens, B.; Trentmann, J.: Climatological analysis of solar and
672 wind energy in Germany using the Grosswetterlagen classification. *Renewable Energy* 2021, 164, 1254-1266,
673 <https://doi.org/10.1016/j.renene.2020.10.102>
- 674 Kaspar, F., Borsche, M., Pfeifroth, U., Trentmann, J., Drücke, J., and Becker, P.: A climatological assessment of balancing
675 effects and shortfall risks of photovoltaics and wind energy in Germany and Europe, *Adv. Sci. Res.*, 16, 119–128,
676 <https://doi.org/10.5194/asr-16-119-2019>, 2019.
- 677 Alexandri, G., Georgoulas, A. K., Zanis, P., Katragkou, E., Tsikerdekis, A., Kourtidis, K., and Meleti, C.: On the ability of
678 RegCM4 regional climate model to simulate surface solar radiation patterns over Europe: an assessment using satellite-based
679 observations, *Atmos. Chem. Phys.*, 15, 13195–13216, <https://doi.org/10.5194/acp-15-13195-2015>, 2015.
- 680 Pelosi, A.; Belfiore, O.R.; D'Urso, G.; Chirico, G.B. Assessing Crop Water Requirement and Yield by Combining ERA5-
681 Land Reanalysis Data with CM-SAF Satellite-Based Radiation Data and Sentinel-2 Satellite Imagery. *Remote Sens.* 2022, 14,
682 6233. <https://doi.org/10.3390/rs14246233>
- 683 Urraca, R., Sanz-Garcia, A., Sanz-Garcia, I., 2020. BQC: A free web service to quality control solar irradiance measurements
684 across Europe. *Sol. Energy* 211, 1–10. <https://doi.org/10.1016/j.solener.2020.09.055>.
- 685 Urraca, R., Gracia-Amillo, A.M., Huld, T., Martinez-de-Pison, F.J., Trentmann, J., Lindfors, A.V., Riihelä, A., Sanz-Garcia,
686 A., 2017. Quality control of global solar radiation data with satellite-based products. *Sol. Energy* 158, 49–62.
687 <https://doi.org/10.1016/j.solener.2017.09.032>.
- 688 Mayer, B.; Kylling, A. Technical note: The libRadtran software package for radiative transfer calculations description and
689 examples of use. *Atmos. Chem. Phys.* 2005, 5, 1855–1877.
- 690 Mueller, R.; Matsoukas, C.; Gratzki, A.; Hollmann, R.; Behr, H. The CM-SAF operational scheme for the satellite based
691 retrieval of solar surface irradiance—A LUT based eigenvector hybrid approach. *Remote Sens. Environ.* 2009, 113, 1012–1022.



- 692 Mueller, R.; Behrendt, T.; Hammer, A.; Kemper, A. A new algorithm for the satellite-based retrieval of solar surface irradiance
693 in spectral bands. *Remote Sens.* 2012, 4, 622–647.
- 694 Hammer, A.; Heinemann, D.; Hoyer, C.; Kuhlemann, R.; Lorenz, E.; Mueller, R.; Beyer, H. Solar energy assessment using
695 remote sensing technologies. *Remote Sens. Environ.* 2003, 86, 423–432.
- 696 Müller, R. and Pfeifroth, U.: Remote sensing of solar surface radiation – a reflection of concepts, applications and input data
697 based on experience with the effective cloud albedo, *Atmos. Meas. Tech.*, 15, 1537–1561, [https://doi.org/10.5194/amt-15-](https://doi.org/10.5194/amt-15-1537-2022)
698 [1537-2022](https://doi.org/10.5194/amt-15-1537-2022), 2022.
- 699 Farnebäck, G. (2003). Two-Frame Motion Estimation Based on Polynomial Expansion. In: Bigun, J., Gustavsson, T. (eds)
700 Image Analysis. SCIA 2003. Lecture Notes in Computer Science, vol 2749. Springer, Berlin, Heidelberg.
701 https://doi.org/10.1007/3-540-45103-X_50
- 702 Ineichen, P. A broadband simplified version of the Solis clear sky model, *Solar Energy*, 2008, 82 (8), 758-762,
703 <https://doi.org/10.1016/j.solener.2008.02.009>
- 704 Antonanzas-Torres, F.; Urraca, R.; Polo, J., Perpiñán-Lamigueiro, O. and Escobar, R. Clear sky solar irradiance models: A
705 review of seventy models, *Renewable and Sustainable Energy Reviews*, 2019, 107, 374-387,
706 <https://doi.org/10.1016/j.rser.2019.02.032>
- 707 Mueller, R.; Pfeifroth, U.; Traeger-Chatterjee, C. Towards Optimal Aerosol Information for the Retrieval of Solar Surface
708 Radiation Using Heliosat. *Atmosphere* 2015, 6, 863-878. <https://doi.org/10.3390/atmos6070863>
- 709 Diekmann, F.J.; Happ, S.; Rieland, M.; Benesch, W.; Czeplak, G.; Kasten, F. An operational estimate of global solar irradiance
710 at ground level from METEOSAT data: Results from 1985 to 1987. *Met. Rdsch.* 1988, 41, 65–79.
- 711 Driemel, A., Augustine, J., Behrens, K., Colle, S., Cox, C., Cuevas-Agulló, E., Denn, F. M., Duprat, T., Fukuda, M., Grobe,
712 H., Haeffelin, M., Hodges, G., Hyett, N., Ijima, O., Kallis, A., Knap, W., Kustov, V., Long, C. N., Longenecker, D., Lupi, A.,
713 Maturilli, M., Mimouni, M., Ntsangwane, L., Ogihara, H., Olano, X., Olefs, M., Omori, M., Passamani, L., Pereira, E. B.,
714 Schmithüsen, H., Schumacher, S., Sieger, R., Tamlyn, J., Vogt, R., Vuilleumier, L., Xia, X., Ohmura, A., and König-Langlo,
715 G. 2018. Baseline Surface Radiation Network (BSRN): structure and data description (1992–2017), *Earth Syst. Sci. Data*, 10,
716 1491-1501, doi:10.5194/essd-10-1491-2018.
- 717 Wild, M., Ohmura, A., Schär, C., Müller, G., Folini, D., Schwarz, M., Hakuba, M.Z., Sanchez-Lorenzo, A., 2017. The Global
718 Energy Balance Archive (GEBA) version 2017: a database for worldwide measured surface energy fluxes. *Earth System*
719 *Science Data* 9, 601–613. <https://doi.org/10.5194/essd-9-601-2017> Wild, M., Ohmura, A., Schär, C., Müller, G., Folini, D.,
720 Schwarz, M., Hakuba, M.Z., Sanchez-Lorenzo, A., 2017. The Global Energy Balance Archive (GEBA) version 2017: a
721 database for worldwide measured surface energy fluxes. *Earth System Science Data* 9, 601–613. [https://doi.org/10.5194/essd-](https://doi.org/10.5194/essd-9-601-2017)
722 [9-601-2017](https://doi.org/10.5194/essd-9-601-2017)
- 723 van den Besselaar, E. J. M., Sanchez-Lorenzo, A., Wild, M., Klein Tank, A. M. G., and de Laat, A. T. J. (2015), Relationship
724 between sunshine duration and temperature trends across Europe since the second half of the twentieth century, *J. Geophys.*
725 *Res. Atmos.*, 120, 10,823–10,836, doi:[10.1002/2015JD023640](https://doi.org/10.1002/2015JD023640).
- 726 Kothe S, Hollmann R, Pfeifroth U, Träger-Chatterjee C, Trentmann J. The CM SAF R Toolbox—A Tool for the Easy Usage
727 of Satellite-Based Climate Data in NetCDF Format. *ISPRS International Journal of Geo-Information.* 2019; 8(3):109.
728 <https://doi.org/10.3390/ijgi8030109>
- 729 Niermann, D., Borsche, M., Kaiser-Weiss, A., Kaspar, F. (2019). Evaluating renewable-energy-relevant parameters of
730 COSMO-REA6 by comparison with satellite data, station observations and other reanalyses. *Meteorologische Zeitschrift*,
731 28(4), 347-360. DOI: [10.1127/metz/2019/0945](https://doi.org/10.1127/metz/2019/0945)
- 732 Bento, V., 2016: Improving Land Surface Temperature retrievals over mountainous regions, Poster presented at the DUE
733 GlobTemperature User Consultation Meeting #4, Lisbon, June 2016.



- 734 Karlsson, K.-G., Stengel, M., Meirink, J. F., Riihelä, A., Trentmann, J., Akkermans, T., Stein, D., Devasthale, A., Eliasson,
735 S., Johansson, E., Håkansson, N., Solodovnik, I., Benas, N., Clerbaux, N., Selbach, N., Schröder, M., and Hollmann, R.:
736 CLARA-A3: The third edition of the AVHRR-based CM SAF climate data record on clouds, radiation and surface albedo
737 covering the period 1979 to 2023, *Earth Syst. Sci. Data*, <https://doi.org/10.5194/essd-2023-133>, 2023.
738 Vernier, J.-P., et al. (2011), Major influence of tropical volcanic eruptions on the stratospheric aerosol layer during the last
739 decade, *Geophys. Res. Lett.*, 38, L12807, doi:[10.1029/2011GL047563](https://doi.org/10.1029/2011GL047563).
740 Roesch, A., Wild, M., Ohmura, A., Dutton, E. G., Long, C. N., and Zhang, T.: Assessment of BSRN radiation records for the
741 computation of monthly means, *Atmos. Meas. Tech.*, 4, 339–354, <https://doi.org/10.5194/amt-4-339-2011>, 2011.
742 Klein Tank, A.M.G. and Coauthors, 2002. Daily dataset of 20th-century surface air temperature and precipitation series for
743 the European Climate Assessment. *Int. J. of Climatol.*, 22, 1441-1453.
744 Alados, I., Foyo-Moreno, I., Alados-Arboledas, L., 1995. Photosynthetically active radiation: measurements and modelling.
745 *Agricultural and Forest Meteorology* 78 (1996), 121-131.